Quaternary Science Reviews 248 (2020) 106565

Contents lists available at ScienceDirect

Quaternary Science Reviews

journal homepage: www.elsevier.com/locate/quascirev

Life on the ice-edge: Paleoenvironmental significance of the radiolarian species *Amphimelissa setosa* in the northern hemisphere

Iván Hernández-Almeida [a, *], K.R. Bjørklund [b], P. Diz [c], S. Kruglikova [d], T. Ikenoue [e], A. Matul [d], M. Saavedra-Pellitero [f], N. Swanberg [g]

[a] Climate Geology, Department of Earth Sciences, ETH Zurich, Sonneggstrasse 5, 8092, Zurich, Switzerland
[b] Natural History Museum, Department of Geology, University of Oslo, P.O. Box 1172 Blindern, 0318, Oslo, Norway
[c] Departamento de Geociencias Marinas, Facultade de Ciencias, Universidade de Vigo, Campus Lagoas-Marcosende S/n, Vigo, 36310, Spain
[d] P.P. Shirshov Institute of Oceanology, Russian Academy of Sciences, Nakhimovsky Prospect 36, 117883, Moscow, Russia
[e] Central Laboratory, Marine Ecology Research Institute, 300 Iwawada, Onjuku-machi, Isumi-gun, Chiba, Japan
[f] School of Geography, Earth and Environmental Sciences, University of Birmingham, United Kingdom
[g] 990 Shenandoah Ave Deltona, FL, 32725-7423, USA

ARTICLE INFO

Article history:
Received 8 July 2020
Received in revised form
24 August 2020
Accepted 24 August 2020
Available online 14 September 2020

Keywords:
Radiolaria
Amphimelissa setosa
Ice-edge
Northern hemisphere
Paleoecology
Proxy

ABSTRACT

The high-latitude Northern Hemisphere is a key region in the global climate balance. Variations in sea-ice extent affect biological productivity, CO_2 exchange and carbon drawdown. Marine proxies indicative of proximity of the ice-marginal zone are therefore essential to understand these processes. *Amphimelissa setosa* is nowadays a dominant radiolarian species in the Arctic basin and very abundant in the high-latitude North Atlantic. This species, now absent from the North Pacific, has been widely used as a qualitative proxy of modern and past environmental conditions in the high-latitude Northern Hemisphere. Using our new and published data on the distribution of *A. setosa* in plankton, sediment trap, surface sediment and downcore samples, we provide a quantitative ecological context for the occurrence of this species. We find that the optimal depth and season of *A. setosa* in the modern North Atlantic and the Chukchi Sea are 160 m and the late boreal summer/early fall (August–October), respectively. A regression model combining environmental variables (temperature, salinity, silicate and chlorophyll-*a* concentrations, apparent oxygen utilization, sea-ice) at that season and depth, are able to explain 43% of the distribution of this species in surface sediments. Based on these new findings, we conclude that the presence of *A. setosa* in surface sediments is closely related to high primary production in the proximity of the sea-ice and areas of ice rafting. The onset of this species started at ca. 1.5 Ma in the North Pacific, linked to a gradual cooling, increased silica availability and southward advance of the ice-margins since the Early Pleistocene. *Amphimelissa setosa*'s decline in this region was likely caused by the development of a quasi-permanent halocline, perennial sea-ice and depletion of silica during marine isotope stage 4. In the high-latitude North Atlantic, the relative abundance of *A. setosa* appears to be related to cooling and supply of dissolved silica from the continent during ice-rafting events. The comprehensive approach taken in this study suggest that *A. setosa* is a useful proxy to explore past variations in the ice-cover in the high-latitude Northern Hemisphere.

1. Introduction

The polar and subpolar realms in the Atlantic sector of the Northern Hemisphere are essential for the heat balance of the global climate system, because they regulate the renewal of deep ocean waters and carbon fluxes (Dickson and Brown, 1994; Ishii et al., 2014). Changes in ice-sheet and sea-ice extent in these regions are key in the global energy balance (Bitz et al., 2006; Ingram et al., 1989), and minor variations in their extension can shift the climate system towards a warm or cold climate mode (Clark et al., 1999; Gildor and Tziperman, 2000). Decline of the ice-covered regions in the Arctic is one of the most striking consequences of the recent anthropogenic climate warming (Stroeve et al., 2007). Satellite and historical in-situ observations provide limited temporal

* Corresponding author.
E-mail address: ivan.hernandez@erdw.ethz.ch (I. Hernández-Almeida).

https://doi.org/10.1016/j.quascirev.2020.106565

resolution (<150 years) (Titchner and Rayner, 2014) to fully understand the sensitivity of the ice-cover to rising temperatures and to foresee response of arctic ecosystems. Climate archives found in the sediment record, such as microfossils from marine microplankton, allow exploration of the natural climate variations and to have a long-trend term perspective of the changes in this ecosystem. Knowledge of the modern biogeography and ecology of those marine plankton organisms and of their relationships to the ice ecosystem is crucial to use these proxies as tracers of past sea-ice.

Radiolarians (siliceous marine protist zooplankton) are significant components in the sediment record at high-latitudes, where carbonate microfossils are rarely preserved due either to dissolution or dilution by other sedimentary phases (Dittert et al., 1999). As such, they are one of the main indicators of past oceanographic conditions in these areas. The polycystine nassellarian *Amphimelissa setosa* is a radiolarian species that dominates radiolarian assemblages in the marginal Chukchi and Beaufort Seas in the Arctic Ocean (Dolan et al., 2014; Ikenoue et al., 2015, 2019), characterized by the presence of seasonal sea-ice (Fig. 1A). This species is also very common in different parts of the high-latitude North Atlantic, such as the Norwegian, Greenland, Iceland and Labrador Seas (Bjørklund et al., 1998; Bjørklund and Kruglikova, 2003; Molina-Cruz, 1991; Molina-Cruz and Bernal-Ramírez, 1996; Swanberg and Bjørklund, 1987b). Several publications have attempted to characterize the ecological potential of this species using surface sediment samples (Bjørklund and Kruglikova, 2003; Cortese et al., 2003; Kruglikova et al., 2007; Matul and Yushina, 1999; Matul, 1989; Matul and Mohan, 2017; Molina-Cruz and Bernal-Ramírez, 1996; Swanberg and Bjørklund, 1992), sediment traps (Ikenoue et al., 2015; Schröder-Ritzrau, 1995) and plankton tows (Bjørklund and Swanberg, 1987; Ikenoue et al., 2015, 2019; Swanberg and Bjørklund, 1987b; Swanberg and Eide, 1992). Different biotic and abiotic factors have been invoked as drivers of *A. setosa* modern distribution including mixing in the water column (Matul and Abelmann, 2005), temperature (Cortese et al., 2003; Molina-Cruz and Bernal-Ramírez, 1996), sea-ice, chlorophyll-*a* and silica concentrations (Dolan et al., 2014; Ikenoue et al., 2015, 2019; Swanberg and Eide, 1992) and fraction of sea-ice meltwater in the surface waters (Ikenoue et al., 2019). However, there is no quantitative determination on what are the main ecological drivers in its present-day and past distribution. The lack of consensus on which are the main ecological drivers of *A. setosa* distribution calls for a re-analysis of existing observations and an adequate synthesis using a systematic and quantitative approach, which may allow a better understanding of *A. setosa* as a potential environmental proxy. In addition, this species shows intraspecific morphological variability, displaying different shell patterns between samples from open ocean and fjord populations (Bjørklund and Swanberg, 1987; Swanberg and Bjørklund, 1987a), and size variability patterns between fossil individuals in the subarctic North Pacific and North Atlantic (Bjørklund et al., 2015; Bjørklund and Kruglikova, 2003; Matul and Abelmann, 2005). This suggests that a complex set of environmental factors are playing an important role in the shell architecture.

Amphimelissa setosa was very common in the high-latitude North Pacific and its marginal seas since the Early Pleistocene, occurring in higher abundances during interglacial and deglacial periods (Ikenoue et al., 2016; Matsuzaki and Suzuki, 2018; Matul and Abelmann, 2005; Matul et al., 2002a; Okazaki et al., 2005), but it disappeared from the region between marine isotope stage (MIS) 5 and 4 (ca. 64–85 ka) (Matul and Abelmann, 2005). The reasons why *A. setosa* is no longer present in the North Pacific remain unresolved. By contrast, in the North Atlantic, the First occurrence (FO) of this species is recorded during MIS 11 (Bjørklund et al., 2015) with higher abundances in glacial intervals (Bjørklund et al., 2015, 2019; Matul, 1995; Matul and Abelmann, 2005; Matul and Yushina, 1999; Matul et al., 2002b).

In this study, we use new and published plankton net and sediment trap data to characterize the optimum living depth and seasonal distribution of this species in the North Atlantic and the Arctic. We determine the best subset of variables that explains its distribution using multiple linear regressions in core-top data. We use this information to re-interpret the *A. setosa* records in both the North Atlantic and North Pacific basins as well as to infer the potential factors influencing the disappearance of *A. setosa* from the high-latitude North Pacific basin. We also compare various size measurements in modern and fossil *A. setosa* individuals from the North Atlantic and North Pacific basins to evaluate whether there are significant environmental pressures or different genetic populations related to the isolation of *A. setosa* in different regions.

2. Material and methods

2.1. Modern and fossil sedimentary datasets

We compiled the relative abundance on *A. setosa* in surface sediments from ten different sources (Supplementary Table 1) distributed among the Greenland, Iceland, Norwegian Seas, and high-latitude North Atlantic, including the Labrador Sea, and Arctic Oceans (Chukchi and Beaufort Seas) ($n = 201$) (Fig. 1A) covering the current spatial distribution of this species. Although some studies have reported trace abundances of *A. setosa* in both surface sediments and in the water column in the North Pacific, we consider these to be misidentifications or reworked individuals (see further explanations in Supplementary Material 1), and therefore they have not been included in this study.

We used sediment trap data with relative abundance of *A. setosa* from four studies, three in the North Atlantic (Schröder-Ritzrau, 1995) and one in the Arctic Ocean (Ikenoue et al., 2015) (Fig. 1B). Each sediment trap data yielded nearly one year of continuous data, with a sampling interval from 10 to 20 days (Table 1), which is suited for accurate determination of temporal occurrence of this species. Regarding the plankton tows, we include five stations in the Chukchi and Beaufort Seas (Ikenoue et al., 2015; Itaki, 2003) and twelve in the Greenland and Iceland Seas (this study) (Fig. 1B), with stratified plankton samples taken at different depth intervals between 500 and 0 m (Table 2). The new plankton net datasets from Greenland Sea correspond to samples taken during the Arctic expeditions ARK VI/1–2 of RV "Polarstern" in 1989 (Krause et al., 1991). Methods for the analyses of these samples are described in Swanberg and Eide (1992). Samples were taken using Hydrobios stratified vertical multi-nets of 63 μm mesh size. Material recovered was dried at low-temperature, and mounted on microscope slides to count radiolaria. In all cases, whenever possible, at least 300 radiolarians were counted. We also used data on the relative abundance of polar planktonic foraminifera *Neogloboquadrina pachyderma* sinistral (Siccha and Kucera, 2017), ice-rafted debris (IRD) (Pirrung et al., 2002), and organic biomarker $\%C_{37:4}$ (Rosell-Melé, 1998) in surface sediments from the Greenland, Iceland and Norwegian Seas. We interpolated these datasets to obtain the value of the aforementioned proxies at the location of the radiolarian surface sediment samples using the weighted-average gridding method included in the ODV software (Schlitzer, 2015).

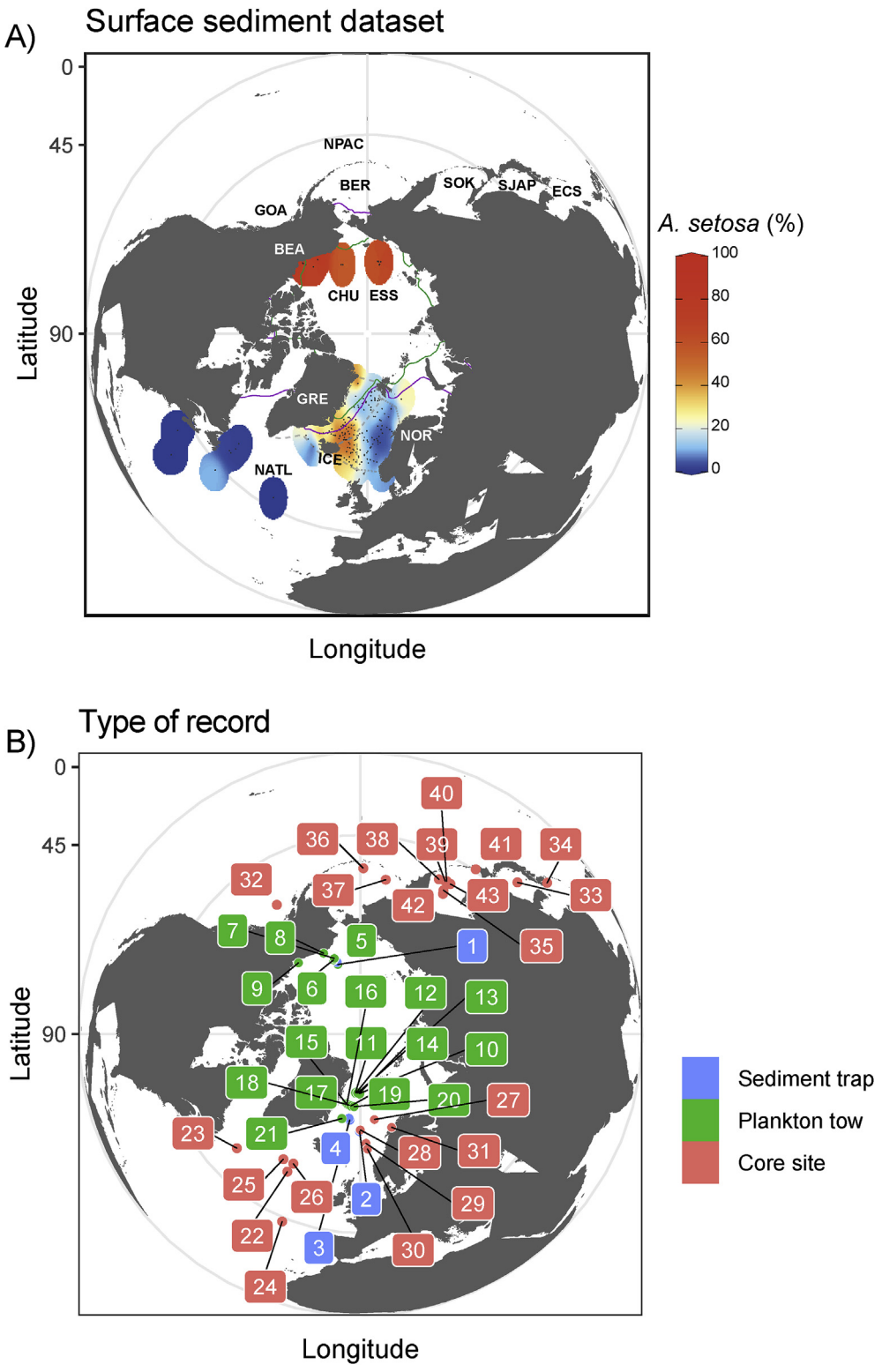

Fig. 1. Map of the high-latitude Northern Hemisphere. (A) Relative abundance of *A. setosa* (%) in surface sediments. Data was interpolated using the weighted-average gridding method in Ocean Data View (ODV) version 4 (Schlitzer, 2015). BEA: Beaufort Sea; BER: Bering Sea; CHU: Chukchi Sea; ECS: East China Sea; ESS: East Siberian Sea; GOA: Gulf of Alaska; GRE: Greenland Sea; ICE: Iceland Sea; NOR: Norwegian Sea; SJAP: Sea of Japan; SOK: Sea of Okhotsk; NATL: North Atlantic; NPAC: North Pacific. Coordinates and references of the surface sediment data set are shown in Supplementary Table 1. Green and purple lines represent >50% of December and August ice-covered area, respectively, based on monthly climatology from Walsh (1978), as included in ODV (Schlitzer, 2015). (B) Location of sediment traps, plankton tows and core sites with *A. setosa* relative abundance data. Details of each code number sample are given in Tables 1–3 (For interpretation of the references to colour in this figure legend, the reader is referred to the Web version of this article.)

Table 1
References, location sampling interval and depth of the sediment trap samples. [a]Same sediment trap samples, different sampling interval.

Code	Station	Reference	Region	Longitude (E)	Latitude (N)	Depth (m)	Mooring depth (m)	Standard sampling interval (days)	Sampling interval
1	Nap10/ 11tupper[a]	Ikenoue et al. (2015)	Chukchi Sea	−162	75	1975	184–260	10–15	04.10.2010–28.09.2011/04.10.2011 –18.09.2012
2	NB6	Schröder-Ritzrau (1995)	Norwegian Sea	−0.46	69.69	3292	500-1000-3000	20	06.08.1991–07.07.1992
3	OG3	Schröder-Ritzrau (1995)	Greenland Sea	−7.04	72.01	2499	500-1000-2300	17–20	15.07.1989–01.08.1990
4	OG5	Schröder-Ritzrau (1995)	Greenland Sea	−7.71	72.38	2624	500-1000-2300	20	06.08.1991–10.07.1992

Table 2
References, location, depth interval for the stratified plankton net samples and average living depth of *A. setosa* at each station.

Code	Station	Reference	Region	Longitude (E)	Latitude (N)	Upper-Lower depths (m)	Average living depth (m)
5	32	Ikenoue et al. (2015)	Chukchi Sea	−161.9	74.5	0–1000	167.3
6	56	Ikenoue et al. (2015)	Chukchi Sea	−160	73.8	0–1000	179.38
7	A00-042	Itaki et al. (2003)	Chukchi Sea	−160.92	73.56	0–500	140.79
8	A00-005	Itaki et al. (2003)	Chukchi Sea	−155.49	71.69	100–260	230
9	A00-022	Itaki et al. (2003)	Beaufort Sea	−138.93	70.48	0–500	138.43
10	A3	This study	Greenland Sea	−1	77.75	0–500	120.12
11	B2	This study	Greenland Sea	−4.75	77.92	0–500	82.56
12	B3	This study	Greenland Sea	−4.13	77.85	0–500	87.8
13	B4	This study	Greenland Sea	−2.8	77.85	0–500	175
14	B5	This study	Greenland Sea	−1.03	77.82	0–500	129.88
15	D1	This study	Greenland Sea	−11.53	75.36	0–500	121.91
16	D2	This study	Greenland Sea	−10.89	75.33	0–500	170.03
17	D3	This study	Greenland Sea	−10.09	75.23	0–500	193.31
18	D4	This study	Greenland Sea	−8.88	75.13	0–500	86.24
19	D5	This study	Greenland Sea	−7.53	75.02	0–500	267.65
20	D6	This study	Greenland Sea	−5	74.96	0–500	246.52
21	G1	This study	Greenland Sea	−12.32	72.06	0–500	194.69
	Average						160.68

We obtained downcore *A. setosa* data from 10 cores in the North Atlantic, and 12 in the North Pacific and marginal seas, including an additional site with unpublished data (SO201-2-77 KL) in the Sea of Okhotsk (Fig. 1B; Table 3). The sites in the high-latitude North Pacific are distributed between the Sea of Japan, Sea of Okhotsk, Bering Sea and Gulf of Alaska. In the North Atlantic, cores were located in the Labrador Sea, south of Iceland, and the mid-latitude North Atlantic, as well as Nordic Seas. The spatial distribution of these sites, from coastal areas to open ocean, is ideal to track paleoenvironmental changes in both the North Pacific and the North Atlantic, such as shifts in the polar fronts or ice-sheet delivery to the ocean. Samples for micropaleontological analyses at Site SO201-2-77 KL were prepared following preparation technique described by Abelmann (1988) and Abelmann et al. (1999), using the sediment fraction of >40 μm. We used the previously published age-models for each site (Table 3).

We additionally employed published size measurements on fossil (downcore) and modern (water column and surface sediment samples) *A. setosa* individuals from the North Atlantic and the North Pacific in order to study whether there were morphotypes that are typical of a particular region or related to specific environmental conditions. Although data stem from different publications, methodology for size measurements was consistent throughout all the studies, with morphological analyses performed on 30 individuals per sample (Bjørklund et al., 2015; Bjørklund and Swanberg, 1987; Matul and Abelmann, 2005). Cephalis height and width, and sagittal diameter were considered, and used for comparison purposes. Total height was also available, but it was discarded from our study data set because the bottom rim is fragile and can break off easily (Bjørklund, personal communication), potentially providing misleading information.

2.2. Estimation of seasonality and depth habitat of Amphimelissa setosa

Living radiolarians inhabit a wide range of depths in the water column, from near the surface to hundreds of meters depth (Boltovskoy, 2017). *Amphimelissa setosa* has been observed in higher abundance at sub-surface depths (90–250 m) in plankton tows (Ikenoue et al., 2015; Itaki, 2003). We calculated the average living depth (ALD) of *A. setosa* in all stratified plankton tows following Rebotim et al. (2017), as the average of the mean depths of the sampling intervals where the species occurred, weighted by the species concentration in those intervals (individuals cm^{-3}). The combination of vertical plankton tow profiles with different spatial resolution in sampling intervals introduces some noise, but still provides a reliable overall estimate of the ALD (Greco et al., 2019). Because data of living radiolarians are not available for all the stations, our calculation of ALD is based on total radiolarians counts (living and dead). We estimated the preferred reproductive season of *A. setosa* based on the highest flux in the sediment traps studies in the Arctic (Ikenoue et al., 2015) and the Greenland, Iceland and Norwegian Seas (Schröder-Ritzrau, 1995).

2.3. Environmental data

Sea surface temperature (SST), salinity (Sal), apparent oxygen utilization (AOU), oxygen concentration (O) and the nutrient concentration of phosphate (Phos), silicate (Sil) and nitrate (Nit), were extracted from the corresponding mean ALD of all the plankton tows and preferred season using the 1 × 1° resolution World Ocean Database 2013 (WOD13) (Garcia et al., 2013; Locarnini et al., 2013; Zweng et al., 2013) and interpolated to the location of the surface

Table 3
References, location and proxies available for the sediment cores with *A. setosa* relative abundance. [a]Additional proxy data correspond to neighbouring Site MD01-2414 (53.1°N, 149.5°E; 90 km away from MD01-2415). [b]Still present in this region. [c]FCO not determined in this core. (FCO: First Common Occurrence; LO: Last Occurrence).

Code	Site	Reference	Region	Longitude (E)	Latitude (N)	Depth (m)	LO (ka)	FCO (ka)	Additional proxy data
22	U1314	Bjørklund et al. (2015)	North Atlantic	−27.88	56.36	2800	[b]	413.9	IRD. Alvarez-Zarikian et al. (2009)
23	P-172	Matul and Abelmann (2005)	North Atlantic	−47.15	53.32	3420	[b]	[c]	
24	L-254	Matul et al. (2002b)	North Atlantic	−22.6	43.78	3950	[b]	[c]	
25	MK-340	Matul and Yushina (1999)	North Atlantic	−31.52	58.51	1699	[b]	[c]	
26	MK-316	Matul (1994)	North Atlantic	−27.28	58.74	2155	[b]	[c]	
27	GIK23259-2	Schröder-Ritzrau (1995)	Norwegian Sea	9.26	72.03	2518	[b]	[c]	*N. pachyderma sin.* Jensen (1998)
28	GIK23424-3	Schröder-Ritzrau (1995)	Norwegian Sea	−0.06	70.03	3291	[b]	[c]	*N. pachyderma sin.* Jensen (1998)
29	GIK23071-2	Schröder-Ritzrau (1995)	Norwegian Sea	2.9	67.08	1306	[b]	[c]	*N. pachyderma sin.* Jensen (1998)
30	GIK23411-5	Schröder-Ritzrau (1995)	Norwegian Sea	3.51	65.79	290	[b]	[c]	*N. pachyderma sin.* Jensen (1998)
31	JM99-1200	Bjørklund et al. (2019)	Norwegian Sea	18.42	69.5	476	[b]	[c]	PBIP25. Cabedo-Sanz et al. (2013)
32	U1417	Matsuzaki and Suzuki (2018)	Northeast Pacific	−147.1	56.95	4187	75	1480	Coarse sand, C37:4, diatoms, opal. Müller et al. (2018)
33	U1425	Matsuzaki et al. (2018)	Sea of Japan	134	39.3	1908	51.5	1470	
34	U1429	Matsuzaki et al. (2019)	East China Sea	129	31.61	732	254.3	[c]	
35	MD01-2415	Matul et al. (2009)	Sea of Okhotsk	149.96	53.95	822	64	1100	Opal, diol index, IRD. Lattaud et al. (2019)[a]
36	U1341	Ikenoue et al. (2016)	Bering Sea	179	54	2139	42.2	990–980	
37	SO201-2-77 KL	This study	Bering Sea	170.69	56.33	213	61.7	[c]	Opal. Riethdorf et al. (2013)
38	LV28-44-3	Matul and Abelmann (2005)	Sea of Okhotsk	153.1	52.04	684	70.5	[c]	
39	LV28-42-4	Matul and Abelmann (2005)	Sea of Okhotsk	150.99	51.71	1041	73.9	[c]	
40	LV27-8-4	Matul and Abelmann (2005)	Sea of Okhotsk	150.57	51.51	1160	85	[c]	
41	MD01-2412	Matul and Abelmann (2005)	Sea of Okhotsk	145	44.52	1225	75.2	[c]	
42	LV27-5-3	Matul and Abelmann (2005)	Sea of Okhotsk	149.5	54.77	476	72.8	[c]	
43	LV28-41-4	Matul and Abelmann (2005)	Sea of Okhotsk	149.05	51.67	1082	94.5	[c]	

sediment samples using weighted average gridding method in ODV v.4 (Schlitzer, 2004). All these data are provided in Supplementary Table 1. In addition, we also extracted seasonal mixed layer depth (MLD) from Monthly Isopycnal & Mixed-layer Ocean Climatology (MIMOC) 2.2 (Schmidtko et al., 2013), and monthly chlorophyll-a (Chlor) data from for the complete period of satellite measurements of the MODIS mission (2003–2016) (https://oceancolor.gsfc.nasa.gov/l3/). Averaged (1871-present) sea-ice concentration was obtained from the 1 ° × 1 ° gridded data set of HADISST (Rayner et al., 2003).

2.4. Statistical analyses

We identify the most important combination of environmental variables explaining statistically the distribution of *A. setosa* in surface sediments. To achieve this, we ran multiple linear models using the relative abundance of this species in surface sediments and the environmental data at preferred growing season of *A. setosa* and ALD (Supplementary Table 1). The criterion to consider the best model is the one with the lowest Akaike's Information Criteria (AIC) number (Akaike, 1973) and lowest Cp statistic of Mallows (Montgomery and Peck, 1992). We used the functions 'regsubsets' (with 'exhaustive' method) and 'stepAIC' (with stepwise search argument as 'both') from the packages 'leaps' (Lumley and Lumley, 2013) and 'MASS' (Ripley et al., 2013), respectively, and 'ggplot2' (Hadley, 2015) for the graph preparation in R version 3.6.0 (R Core Team, 2019).

3. Results and discussion

3.1. Seasonal and vertical habitat of Amphimelissa setosa

The ALD of *A. setosa* in the Greenland and Iceland Seas, ranges between 267 and 82 m, and between 230 and 138 m at five stations in Chukchi and Beaufort Seas (Arctic Ocean). The average ALD of *A. setosa* across the four seas is 160 m (Table 2). Ideally, the environmental variables at the ALD would be more representative to characterize the habitat of *A. setosa*. However, many surface sediments do not have a plankton net sample nearby to infer its ALD, thus we use instead the global mean ALD of 160 m to extract the environmental data. The ALD of *A. setosa* in the Greenland Sea shows the largest variability of all the plankton net data set (267-82 m, see Table 2). This variation in ALD could be due to the competition with other silica organisms. When diatoms are more abundant in the surface layers, silica concentrations decrease due to more efficient uptake by this group, and *A. setosa* finds more suitable conditions (and higher silica concentrations) in deeper layers, where diatoms are absent (Biard and Ohman, 2020). Higher fluxes of *A. setosa* in sediment traps from the Chukchi and Beaufort Seas occur between August and November, while they occur in the Greenland and Norwegian Seas between August and October (Ikenoue et al., 2015; Schröder-Ritzrau, 1995) (Fig. 2). The latter region also shows smaller peaks in *A. setosa* during spring. The slight difference in the timing of the maximum abundance of *A. setosa* between Chukchi and Beaufort Seas, and Norwegian, Greenland, Iceland Seas indicates that the maxima abundance of *A. setosa* is time transgressive, taking place early in the south and later in the north. This is likely related to melting/retreat of sea-ice, as suggested by previous studies (Ikenoue et al., 2015; Swanberg and Eide, 1992) (Fig. 1A). The spring peak could represent early melting of sea-ice at lower latitude locations. Despite this slight offset, the fluxes of *A. setosa* during August–October are on average 1.7 to 3.5 times higher than during the rest of the months in both regions. The result of paired *t*-test (one-tailed) (Excel, Analysis ToolPak) shows that the mean fluxes of this species during August–October are significantly higher (at $p < 0.05$) than the mean fluxes during the rest of the months in which the sediment traps where deployed (Supplementary Material 2). For this reason, we use the August–October months as representative of the most favourable growing period for *A. setosa*.

3.2. Distribution of Amphimelissa setosa in surface sediments

The species *A. setosa* is an Arctic Ocean cold water species, but also occupies areas in the Barents Sea, Nordic Seas, as well as the Labrador Sea (Fig. 1A) bearing warmer temperatures. The

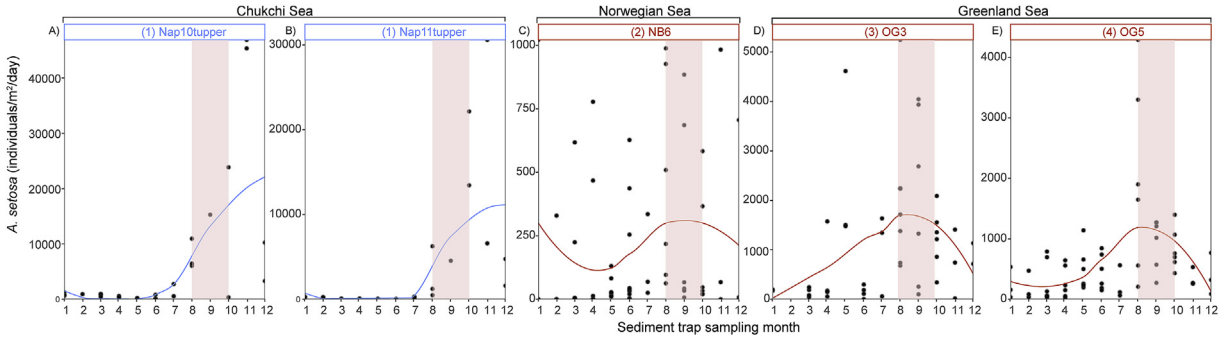

Fig. 2. Fluxes of *A. setosa* (individuals/m^2) versus sampling month in sediment traps from the high-latitude North Atlantic: (A–B) in the Chukchi Sea (Ikenoue et al., 2015), and (C–D) in high-latitude Norwegian, Greenland, and Iceland Seas (Schröder-Ritzrau, 1995). Red and blue lines show locally estimated scatterplot smoothing (loess) (span = 0.9). Vertical red shading indicates months between August–October. Numbers in parenthesis correspond to the code number in Table 1. (For interpretation of the references to colour in this figure legend, the reader is referred to the Web version of this article.)

abundance of *A. setosa* is about 58% in the Chukchi Plateau area, 80% in the Beaufort Sea shelf/slope area, and up to 100% in the East Siberian Sea (Hernandez-Almeida et al., 2020). In the Barents Sea, *A. setosa* is present only west of Novaya Zemlya with abundances up to 77% (Bjørklund and Kruglikova, 2003): the overall numbers of radiolaria are lower than in the Chukchi and Beaufort Seas due to preservation issues. In the Greenland are of the Nordic Seas, this species has a marked preference for cold waters, with abundances above 60% peaking to 76% on the Iceland Plateau (Bjørklund et al., 1998). In general *A. setosa* decreases in abundance eastwards as it meets with and submerges below the inflowing warm Atlantic water in the Nordic Seas, with values between 5 and 10-% close to the west coast of Norway. Lowest values (<5%) are found south of Iceland, and in the Labrador Sea and mid-latitude North Atlantic (Fig. 1A).

3.3. Environmental factors controlling modern Amphimelissa setosa

Understanding the proxy value of a microfossil entails constraining the environmental (physical, chemical and biological) factors that determine its modern distribution. Using environmental data at the season and water depth in which *A. setosa* lives today (August–October and 160 m depth), we ran a multiple linear regression model with all the variables available. The best model explains 43% of the variance in the distribution of *A. setosa* in surface sediments ($R^2_{adj} = 0.43$, $p < 0.05$; lowest AIC = 1212.9 and Cp statistic of Mallows: 6), and includes SST, Sal, AOU and silicate at 160 m, chlorophyll-*a* between August–October and sea-ice concentration (Table 4). The most important contributor to the model is SST (Supplementary Material), while chlorophyll-a is not highly significant ($p > 0.05$), likely due to cofounding with other variables. This analysis reveals that bottom-up factors, such as nutrients, salinity and temperature, are the drivers most significantly associated with the distribution of *A. setosa.* This result is consistent with the study by Biard and Ohman (2020), which highlighted the importance of temperature, deep chlorophyll-*a* maximum and dissolved silica concentration influencing radiolarian populations living between 100 and 200 m depth in the water column. The unexplained variance in *A. setosa* distribution could be caused by the interaction of multiple biotic dependencies (e.g. prey-depredator interactions, symbionts, parasitism) (Biard and Ohman, 2020), or preferential dissolution.

Today, the Norwegian, Greenland and Iceland Seas are well mixed and isohaline areas with lower SST corresponding to deep-water formation occur (Swift and Aagaard, 1981) (Supplementary Figure 1). The importance of temperature for *A. setosa* agrees with previously observed temperature dependence of radiolarian assemblages in culture experiments (Anderson et al., 1988, 1990; Matsuoka and Anderson, 1992) or in field observations (Abelmann et al., 1999; Boltovskoy and Correa, 2016; Cortese et al., 2005; Hernandez-Almeida et al., 2020; Matul and Mohan, 2017).

Amphimelissa setosa is rarely found in the central Arctic Ocean, which is usually covered by perennial sea-ice (Bjørklund and Kruglikova, 2003), or in surface sediments in the proximity of the East Greenland continental shelf, usually covered by winter sea-ice. The absence of *A. setosa* in the same area could also reflect dissolution, as the East Greenland region shows low opal accumulation due to the intermittent perennial ice-cover (Schlüter et al., 2001). Its abundance (up to 78%) increases east of the Kolbeinsey Ridge (16°W), beyond the limits of the winter sea-ice. Swanberg and Eide (1992) found high abundances of juvenile and adult *A. setosa* along the ice-edge east of 16°W in boreal summer in the Greenland Sea, which were characterized by relatively cold temperatures, low salinity, high values of chlorophyll-*a* and phaeopigments. Ikenoue et al. (2019) has suggested that water freshening due to river runoff and sea-ice melting in the Arctic Ocean is an important factor for the proliferation of *A. setosa*, which may influence the main source of food supply for radiolarians. Abundances of *A. setosa* up to 100% are observed in the Chukchi and Beaufort Seas and are related to a cold waters masses along the sea-ice edge during boreal summer (Dolan et al., 2014; Ikenoue et al., 2015, 2019; Itaki et al., 2003). The proximity of the ice-edge causes enhanced vertical mixing which supplies higher concentrations of nutrients (such as nitrate and silicate) than ice-free areas, and stimulates primary productivity (Apollonio, 1973; Assmy et al., 2013).

Interestingly, we find that the silicate concentration at 160 m is a variable significant to the distribution of *A. setosa* in surface sediments. Silica concentration is also correlated with sea-ice concentration ($R = 0.72$, $p < 0.001$, Supplementary Material). In the Beaufort Sea, silica concentrations are generally higher below 100 m, and a mid-depth maximum between 125 and 200 m depth is found at the upper halocline (Varela et al., 2016). Major sources of silica at the surface waters included the Mackenzie River and sea-ice, and Bering Sea waters at the subsurface (Varela et al., 2016). *Amphimelissa setosa* dominates the radiolarian assemblages (up to 100% in the East Siberia Sea) in areas with high concentrations of subsurface silica, suggesting the importance of this nutrient in controlling the species distribution.

It is generally assumed that high dissolved silica content enhances silicification of polycystines and, thus, also controls the distribution of species. However, this has not been observed in short-term laboratory experiments: radiolarian skeletons do not show any significant response to increases in dissolved silica (Sugiyama and Anderson, 1997; Suzuki et al., 2013). Culture

Table 4
Final model statistics, significance of the parameters and AIC of alternative models including (+) or excluding (−) parameters.

Final model = A. setosa ~ Sea-ice + SST Aug–Oct 160 +Sal Aug–Oct 160 + Sil Aug–Oct 160 + AOU SST Aug–Oct 160 + Chlor Aug–Oct					
	Estimate	Std. Error	t value	p	
(Intercept)	−1905.306	708.9287	−2.688	0.007822	**
Sea-ice	−0.5072	0.1464	−3.464	0.000654	***
SST Aug–Oct 160	−7.4988	1.3734	−5.46	1.45E-07	***
Sal Aug–Oct 160	54.6408	20.1539	2.711	0.007306	**
Sil Aug–Oct 160	3.6488	1.1686	3.122	0.002068	**
AOU Aug–Oct 160	39.6691	8.1723	4.854	2.48E-06	***
Chlor Aug–Oct	4.8496	2.6587	1.824	0.069685	.
	Df	Sum of Sq	RSS	AIC	
+Nit Aug–Oct 160	1	345.6	80717	1221.1	
-Chlor Aug–Oct	1	1390.2	82453	1221.3	
+MLD Aug–Oct	1	120.9	80941	1221.6	
+Phos Aug–Oct 160	1	33.9	81028	1221.8	
+O Aug–Oct 160	1	7.1	81055	1221.9	
-Sal Aug–Oct 160	1	3071.4	84134	1225.4	
-Sil Aug–Oct 160	1	4073.8	85136	1227.8	
-Sea-ice	1	5014.9	86077	1230	
-AOU Aug–Oct 160	1	9845.5	90908	1241	
-SST Aug–Oct 160	1	12456.3	93519	1246.7	

Signif. codes: 0 '***' 0.001 '**' 0.01 '*' 0.05 '.' 0.1 ' ' 1.
Residual standard error: 20.44 on 194 degrees of freedom.
Multiple R-squared: 0.4485, Adjusted R-squared: 0.43.
F-statistic: 26.3 on 6 and 194 DF, p-value: < 2.2e-16.
AIC: 1212.9; Cp statistic of Mallows: 6.018518.

experiments with tropical radiolarian species show reduced longevity under high-dissolved silica concentration (up to 150 μM/L) (Sugiyama and Anderson, 1997). However, these culture experiments were only successful for some tropical species and, therefore, we cannot be certain of whether these results can be generalized to all radiolarian species. In more recent experiments using fluorescence methods, which are more sensitive to differences in silicification, it was observed that growth stages of certain polycystine species can produce variations in the skeletal thickness of different parts of the shell (Ogane et al., 2010). Field studies have not shown evidence of any significant relationship between dissolved silica and radiolarian species abundance or degree of silicification so far (Suzuki and Not, 2015). It is feasible that the relationship of subsurface silica and *A. setosa* abundance derives from indirect mechanisms, such as food web processes involving predation on siliceous phytoplankton, as has been observed in other subsurface radiolarian species (Biard and Ohman, 2020). This would also explain the significance of AOU, which is a measure of how much oxygen has been taken up by sea life (Garcia et al., 2009), and chlorophyll-*a*, which are both related to the primary production in the ocean. Dissolved silica is limiting for diatoms, and retreating and melting of the ice-edge in high latitudes make this nutrient available for phytoplankton producers adapted to these conditions (Jin et al., 2007; Syvertsen, 1991), such as some diatoms species (Fryxell, 1989; Weckström et al., 2020) and perhaps radiolarians. In iceberg production areas, it has been observed that ice-sheet meltwaters are exporting large quantities of reactive silica, which could be used by planktonic organisms (Duprat et al., 2016; Hawkings et al., 2017; Hopwood et al., 2020) into the ocean. Diatom blooms, together with high density of radiolarians, have been observed in west-Norwegian fjords covered with sea-ice during winter and receiving glacial meltwater during early spring (Bjørklund, 1974; Bjørklund et al., 2008; Swanberg and Bjørklund, 1986, 1987b). In such cases, a high density of *A. setosa* could indicate a direct or indirect trophic dependency between this radiolarian species and phytoplankton related to glacial meltwater in these fjords.

Besides the significance of SST, Sal, AOU, silica, chlorophyll-*a* and sea-ice for *A. setosa*, the relative abundance of this species shows a positive correlation with IRD concentration ($R = 0.49$, $p < 0.001$), and relative abundance of *N. pachyderma* sin. ($R = 0.46$, $p < 0.001$), $\%C_{37:4}$ ($R = 0.67$, $p < 0.001$) in surface sediments in the high-latitude North Atlantic and marginal basins of the Arctic Ocean (Fig. 3A–C). Because we interpolated the proxy data to the locations of the surface sediment samples with *A. setosa* data, some of the correlation plots show certain concentration of points which do not show correlation to *A. setosa* percentages, for example at high values of *N. pachyderma* sin. (90–100%). Alternatively, this could represent different ecological sensitivities of *A. setosa* to the conditions represented by these proxies. *Neogloboquadrina pachyderma* sin. is the dominant species north of the Arctic front, with percentages up to 90%. This species is able to live below the sea-ice, and shows that the highest absolute abundances along the summer ice margin, parameters which are related to high primary production (Carstens et al., 1997). High abundance of $\%C_{37:4}$ (>5%) in sediments and the water column is associated with the influence of freshwater from sea-ice and/or icebergs in polar and sub-polar waters (Bendle et al., 2005; Harada et al., 2003; Rosell-Melé, 1998; Seki et al., 2005). Deposition of IRD in sediments occurs with the melting of ice (continental and/or sea-ice) (Pirrung et al., 2002; Ruddiman, 1977), which also delivers nutrients to the surface ocean (Apollonio, 1973; Duprat et al., 2016). Therefore, it is reasonable to assume that in the past *A. setosa*'s species-proxy relationships were similar to those of today. We conclude that the combination of late boreal summer/autumn environmental variables, such as SST, sea-ice productivity-related factors, that favour proliferation of *A. setosa*, must have occurred also in the high-latitude North Atlantic and North Pacific in the past, when *A. setosa* was abundant and there were increases in indirect polar indicators such as the abundance of *N. pachyderma* sin., IRD and $\%C_{37:4}$.

3.4. Exploring the morphological variability of Amphimelissa setosa populations

Fossil *A. setosa* individuals in downcore samples from the North

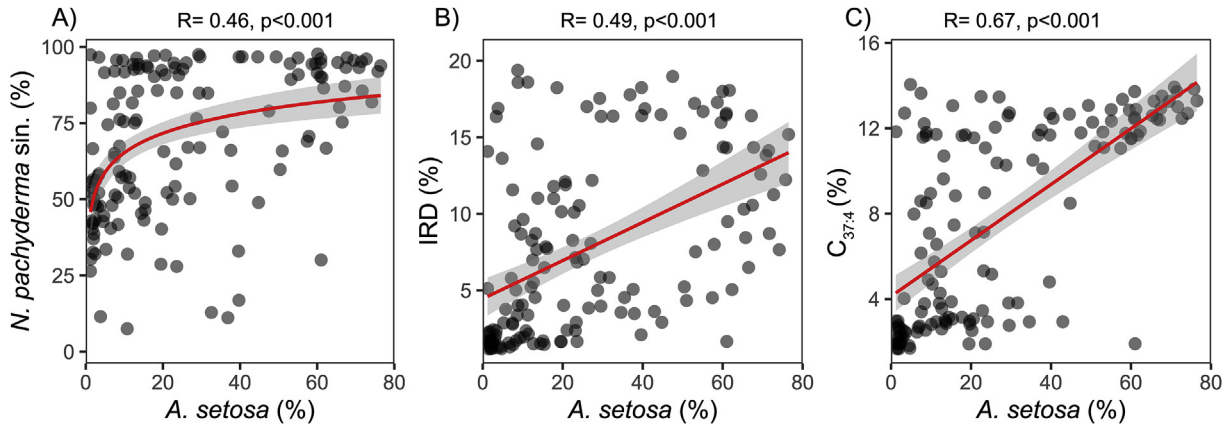

Fig. 3. Correlation between *A. setosa* abundance in surface sediments and abundance of (A) *N. pachyderma* sin. (%) (Siccha and Kucera, 2017), (B) IRD (%) (Pirrung et al., 2002), and (C) $C_{37:4}$ (%) (Rosell-Melé, 1998) in surface sediments in the high-latitude North Atlantic (correlation line in red, standard error in grey). Note that for panel A the fit is logarithmic. Environmental data interpolated with weighted-average gridding method in ODV v.4 (Schlitzer, 2015). (For interpretation of the references to colour in this figure legend, the reader is referred to the Web version of this article.)

Atlantic and the North Pacific basins show some differences in morphological characteristics. Overall, the relationship between cephalis width and height in populations from the two basins have similar slope but different intercepts as shown in Fig. 4A and B. Sea of Okhotsk specimens have significantly larger cephalis width and height (two-samples *t*-test, $p < 0.05$, Supplementary Material) compared to the North Atlantic ones (Fig. 4A and B), while for the sagittal diameter, the differences are not significant. Interestingly, morphological measurements of *A. setosa* for MIS 10 samples (374–337 ka) in Site U1314 are more similar to those in the Sea of Okhotsk, in particular for samples from MIS 11 (424 ka), 9 (337 ka) and 7e (243 ka). *Amphimelissa setosa* appeared in North Atlantic sediment records during transition MIS 11/10, possibly migrating from the North Pacific (Bjørklund et al., 2015). This is indicated by a peak of ~65% at MIS 10/9 transition (347 ka) in Site U1314 (Fig. 5a). The similarity of *A. setosa* size in the Sea of Okhotsk and North Atlantic fossil samples between MIS 11-9 suggests that *A. setosa* populations in the Sea of Okhotsk shared morphological characteristics with the ones that migrated first to the North Atlantic. On the contrary, samples between MIS 4 and 2 had smaller sizes. On glacial/interglacial time-scales, Cortese and Bjørklund (1997) observed differences in size in radiolarian species *Actinomma boreale* in the Norwegian Sea, with the decreasing size from the Younger Dryas towards the Holocene negatively correlated to SST. This is opposite to test size trends observed in surface sediments from the Norwegian Sea (64-62°N; 6-4°E) to the Iceland Plateau (68-66°N; 24 -8°W) where size and July SST were positively correlated. This indicates that not only SST, but other factors such as nutrients and productivity might be responsible for the changes in size in *A. boreale* in the North Atlantic, and the same might apply for skeletal size differences in *A. setosa.*

Measurement of sagittal diameter and cephalis height allows us to distinguish four different groups of samples with similar slopes but different intercepts (Fig. 4C). Plankton and surface sediment samples from the Iceland Plateau show different cephalis widths and sagittal diameter sizes, and both are larger than core samples in

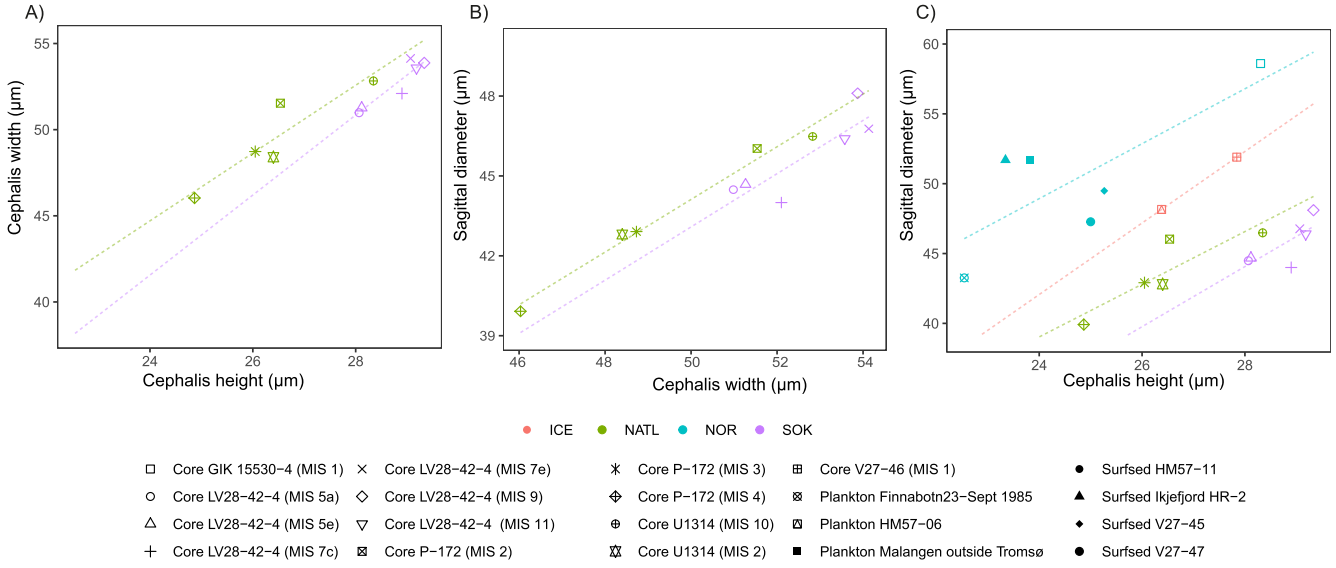

Fig. 4. Biometrics of *A. setosa* in plankton, surface sediment and downcore samples. Terminology of the parameters measured follows that of Matul and Abelmann (2005). (A) Cephalis height vs Cephalis width, (B) Cephalis width vs sagittal diameter, and (C) Cephalis height vs Sagittal diameter. ICE: Iceland Sea; NATL: high-latitude North Atlantic; NOR: Norwegian Sea; SOK: Sea of Okhotsk. Dashed coloured lines indicate the regression line between the two morphological parameters for samples in the same region.

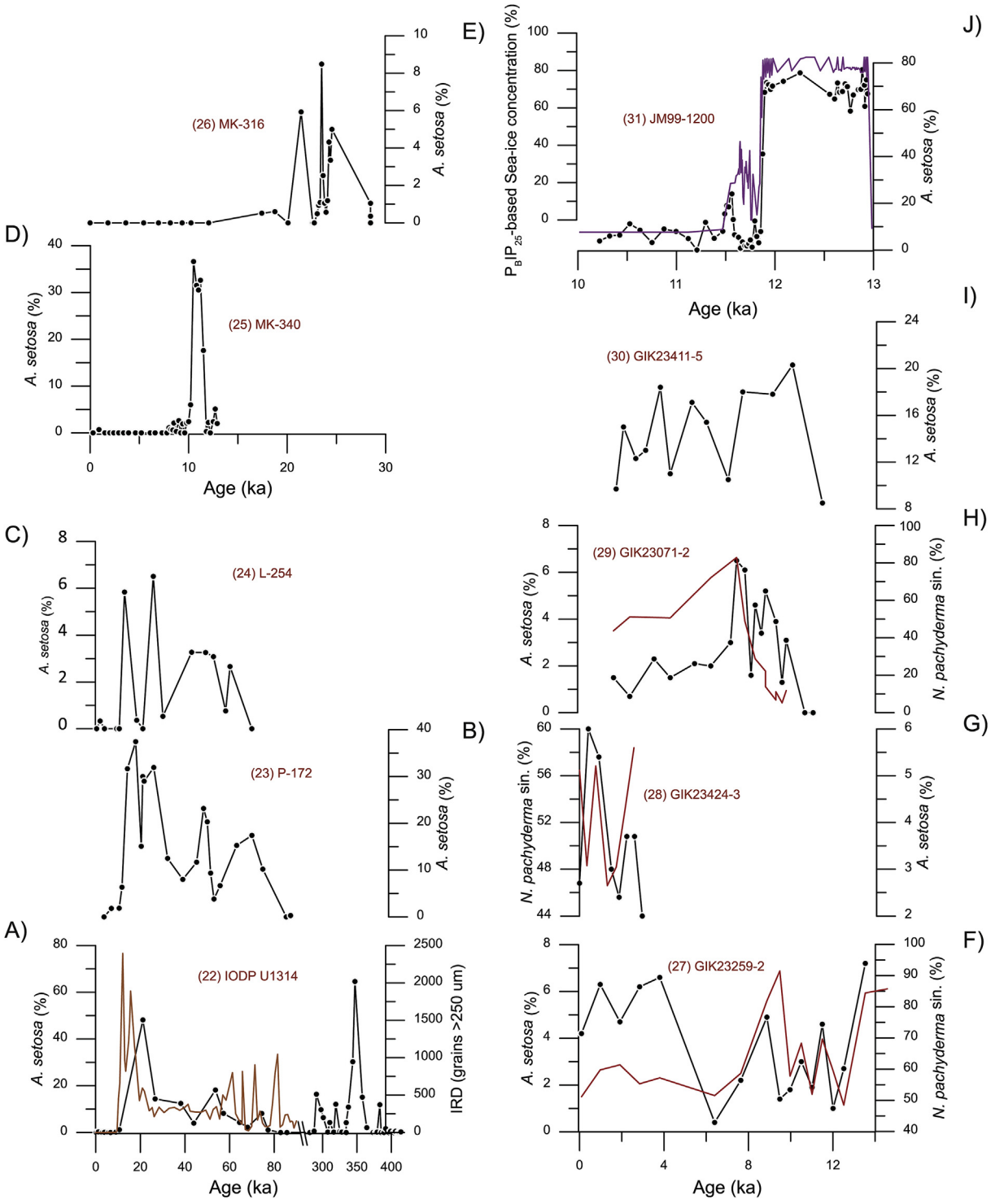

Fig. 5. Downcore relative abundance of *A. setosa* (%) in sediment cores in the high-latitude North Atlantic (left), (A) Site U1314 (Bjørklund et al., 2015) and IRD grains (brown) (Alvarez Zarikian et al., 2009), (B) Site P-172 (Matul and Abelmann, 2005), (C) Site L-254 (Matul et al., 2002b); (D) Site MK-340 (Matul and Yushina, 1999), (E) Site MK-316 (Matul, 1994); and the Nordics Seas (right), (F) Site GIK23259-2 (Schröder-Ritzrau, 1995) and *N. pachyderma* sin. (red) (Jensen, 1998), (IG) GIK23424-3 (Schröder-Ritzrau, 1995) and *N. pachyderma* sin. (red) (Jensen, 1998), (H) Site GIK23071-2 (Schröder-Ritzrau, 1995) and *N. pachyderma* sin. (red) (Schulz, 1995), (I) Site GIK23411-5 (Schröder-Ritzrau, 1995), and (J) Site JM99-1200 (Bjørklund et al., 2019) and seasonal sea-ice concentration (%) (purple) calculated using P_BIP_{25} data (Cabedo-Sanz et al., 2013). Numbers in parenthesis correspond to the code number in Table 3. (For interpretation of the references to colour in this figure legend, the reader is referred to the Web version of this article.)

the North Atlantic (south of Iceland), although they have the same slope. The North Atlantic and Iceland populations fall between the other two, with the Sea of Okhotsk and the Norwegian Sea populations having the smallest and the largest sagittal diameter, respectively. These differences may be due to the genetic plasticity of *A. setosa* in response to the specific environmental characteristics of each region. Bjørklund and Swanberg (1987) identified two morphotypes of *A. setosa*, one with reticulated pore ornamentation

associated with the Norwegian fjords (see images in Supplementary Material 1), and another with a more compact appearance typical of open ocean conditions. They hypothesized the fjord morphotypes to be related to the high temperature (>7 °C), high production, competition for resources, and rapid growth conditions in the fjords. This reticulated form, or "rapid growth" morphotype, was not observed by Swanberg and Eide (1992) in the cold water assemblage close to the ice-edge in Greenland Sea, where the water temperatures were mostly below 0 °C (and summer temperatures between 4 and 5 °C). If both Greenland, Iceland and Norwegian Seas populations of *A. setosa* shared a common arctic ancestor (Bjørklund et al., 2015), the clear differences in skeletal construction (Bjørklund and Swanberg, 1987), and morphology (Fig. 4D) suggest large endemism and genetic plasticity among the populations (sympatric speciation) dwelling in different parts of the North Atlantic Ocean. This process might have been favoured by character displacement during early stages of sympatric speciation (Brown and Wilson, 1956) due to the different environmental conditions at each region and competitive interactions among different radiolarian species.

The ability of *A. setosa* to successfully disperse across different basins for extended periods of time appears to be a common ability in other planktonic organisms (Nelson et al., 2009; Reid et al., 2007; Sexton and Norris, 2008). If geographic isolation persisted over significant periods of time, some genes that control skeletal morphology might change, creating new morphotypes (allopatric speciation) (Norris, 2000). Differences in cephalic size and sagittal diameter between fossil and modern Iceland Plateau, Norwegian Sea and high-latitude North Atlantic populations are clear, and they persist when compared with extinct populations in the Sea of Okhotsk (Fig. 4). This would indicate that genetic drift and allopatric speciation, together with variation in environmental factors (temperature, salinity, food source), may account for some of the observed morphological differences in *A. setosa*, as it has been hypothesized for other radiolarian species belonging to the genus *Actinomma* with similar migration history (Kruglikova et al., 2009). These morphological variations should be further investigated, in particular the size of the cephalis, as they seem to be useful markers to trace past differences in environmental parameters through time.

3.5. Paleoenvironmental significance of A. setosa in core sediments

From the statistical results that show a preference for certain environmental variables at a specific season and depth (August–October, 160 m depth), and the surface distribution patterns of *A. setosa* in the modern Arctic Ocean and Nordic Seas, we argue that the distribution of this species relates to subsurface nutrients (mainly silicate) and temperature at subsurface waters as well as to productivity linked to the proximity of ice-edge. We evaluate the significance of the records of *A. setosa* in multiple sites of the high-latitude Northern Hemisphere across the Pleistocene compared to other independent proxies.

3.5.1. Assessing the relationship of Amphimelissa setosa with meltwater events: analysis of North Atlantic records

The oldest presence of *A. setosa* in the high-latitude North Atlantic and Nordic Seas, migrated from the North Pacific, is recorded at IODP Site U1314 at 413.9 ka during the sea-level high stands at Marine Isotope Stage (MIS) 11, although in very low percentages (Bjørklund et al., 2015). The species rose to 60% during MIS 10 and 9 at Site U1314, reaching also very high percentages in the Labrador Sea and mid-latitude North Atlantic during the same time interval (Bjørklund et al., 2015) (Fig. 5A). The high percentages of *A. setosa* during MIS 10 in the North Atlantic coincide with high abundances of the polar planktonic foraminifera *N. pachyderma* sin. (Johannessen et al., 1994), which occurred together with increased content of IRD in several cores located in the subpolar North Atlantic (Kandiano and Bauch, 2003; St. John et al., 2004). The abundance *A. setosa* decreases between MIS 9 to MIS 4, and increases again from MIS 4 to MIS 2, which coincides with steady higher abundance of IRD (Fig. 5A). The higher IRD content in the North Atlantic during MIS 10, 4 and 2 indicates the collapse and melting of Circum-Atlantic ice-sheets (Alvarez Zarikian et al., 2009). Such meltwater could have supplied large amounts of silicic acid to the ocean, which could have sustained higher primary productivity along the marginal ice zone, promoting the proliferation of high numbers of *A. setosa.* Additionally, sediment cores in the mid and high-latitude North Atlantic, L254, P-172 and MK-340 (Fig. 5B–E), show peaks of *A. setosa*, between 15 and 10 ka, which coincide with higher silica concentration in the ocean supplied by melting glaciers from Greenland (Hawkings et al., 2018). At sites in the Barents Slope (Site GIK23259-2) (Fig. 5F) and Vøring Plateau (Sites GIK23071 and GIK23411-5) (Fig. 5F, H-I), *A. setosa* show increases between 12–8 ka, concurrent with the dominance of *N. pachyderma* sin. (50–70%). This correspondence indicates that these intervals were characterized by the intrusion of cold arctic waters in the Nordic Seas, and potentially the presence of sea-ice in that region (Carstens et al., 1997; Jensen, 1998) (Fig. 5F–H).

The radiolarian record in the core JM99-1200, recovered in Andfjord in northern Norway, shows a rapid transition from high to low *A. setosa* abundances between the Younger Dryas and the Holocene. This also coincides with a reduction in ice-rafted debris, and lower seasonal sea-ice concentration inferred from the organic biomarker-derived proxy P_BIP_{25} (Fig. 5J) (Bjørklund et al., 2019; Cabedo-Sanz et al., 2013). We suggest that higher abundance of *A. setosa* reflects cold SST, seasonal sea-ice, together with higher silicic acid input to the fjord by glacier meltwater. The same has been observed in fjords in Greenland and Svalbard (Halbach et al., 2019; Meire et al., 2016).

3.5.2. The onset of Amphimelissa setosa in the North Pacific

The lineage of *A. setosa* in the family *Cannobotryidae* is unknown and there is no information about any ancestors in the North Pacific. In the Bering Sea, single specimens of *A. setosa* were found at 4–2.4 Ma at Sites U1341 (Ikenoue et al., 2016) and at U1340 (Zhang et al., 2014). The sporadic occurrence of this species in Pliocene and Early Pleistocene sediment records is not robust enough as to be considered a biostratigraphic marker. However, the increase of this species since 1.48 Ma is consistent across different regions in the North Pacific and marginal seas. Therefore, we prefer to use the term First Common Occurrence (FCO) to refer to the earliest common presence of *A. setosa* in the North Pacific, following (Ikenoue et al., 2016). The oldest FCO of *A. setosa* was determined at 1.48 Ma (Fig. 6A) at IODP Site U1417, in the northeastern Pacific (Gulf of Alaska), which is almost the same as for the Sea of Japan, recorded at 1.47 Ma (Kamikuri et al., 2017; Matsuzaki et al., 2018) (Fig. 6D). In the Sea of Okhotsk, the FCO of *A. setosa* was found at 1.1 Ma (Matul and Abelmann, 2005; Matul et al., 2002a) (Fig. 6F), while in the Bering Sea, at 990–980 ka (Ikenoue et al., 2016) (Fig. 6G).

Notably, the FCO of *A. setosa* across the high-latitude North Pacific coincides with an increase in the arctic-water indicator % $C_{37:4}$ at around 1.5–1.1 Ma in the whole basin (IODP sites U1417, U1341 and ODP site 882) (Fig. 6D, H-I) (Horikawa et al., 2015; Martínez-Garcia et al., 2010; McClymont et al., 2008; Müller et al., 2018). Peaks in *A. setosa* abundance at Site U1417 between 1.48 and 1 Myr coincide with higher bio-siliceous primary productivity and IRD activity (Fig. 6A–C). Multi-proxy evidence at Site U1417 indicates that biosiliceous productivity (as seen by opal and diatom

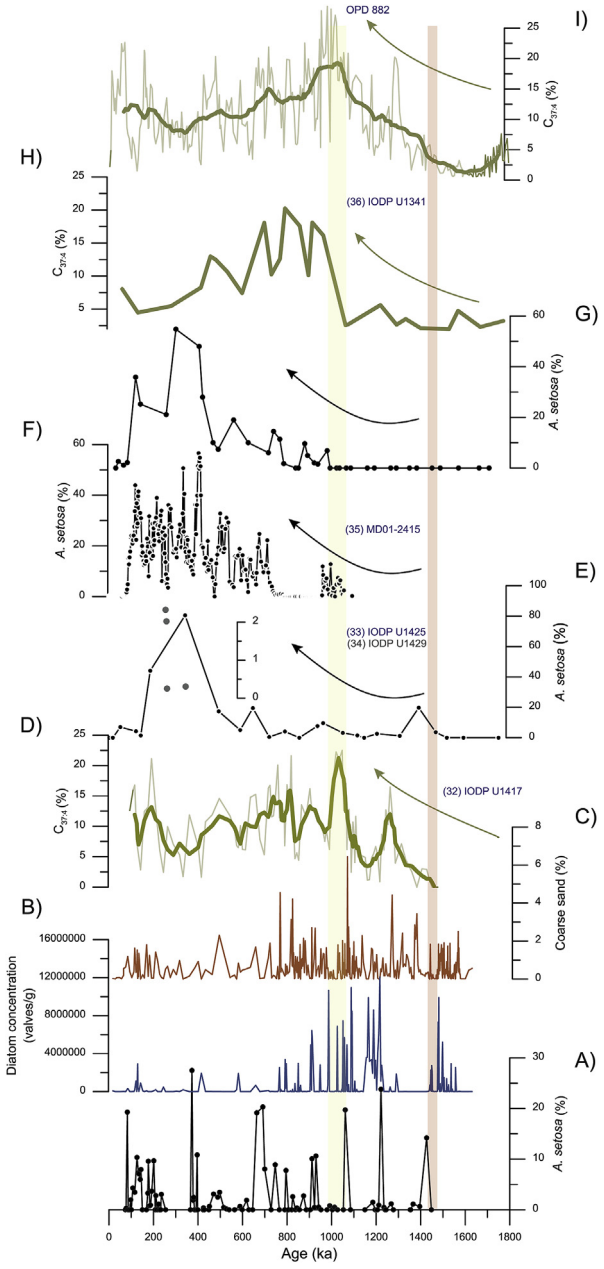

Fig. 6. (A) Downcore relative abundance of *A. setosa* (%) (Matsuzaki and Suzuki, 2018), (B) diatom valve concentration (valves/g), (C) coarse sand content (%), and (D) $C_{37:4}$ (%) (thick line, 5 points running average) (Müller et al., 2018) at IODP Site U1417. (E) Relative abundance of *A. setosa* (%) at IODP Site U1341 (Ikenoue et al., 2016). (F) Relative abundance of *A. setosa* (%) at MD01-2415 (Matul et al., 2009). (G) Relative abundance of *A. setosa* (%) at IODP Site U1425 (lines) (Matsuzaki et al., 2018) and U1429 (dots) (Matsuzaki et al., 2019). (H) Uk'_{37} -SST (°C) and (I) $C_{37:4}$ (%) at ODP Site 882 (50.3°N, 167.5°E) (thick lines, 5 points running average) (Martínez-Garcia et al., 2010; McClymont et al., 2008). Vertical red shading indicates FCO in sites U1417 and U1425 (1.48–1.47 Ma), and yellow vertical shading indicates FCO in sites MD01–2415 and U1341 (1.1–0.98 Ma). Numbers in parenthesis correspond to the code number in Table 3. The sites are ordered chronologically, from the oldest occurrence of *A. setosa* in the North Pacific at the bottom (i.e. U1417), to the youngest one (i.e. U1341) in the upper part. (For interpretation of the references to colour in this figure legend, the reader is referred to the Web version of this article.)

concentration) was strongly controlled by continental dust and ice-rafting processes supplying micro and macro nutrients necessary to stimulate productivity (Müller et al., 2018). The Arctic sea-ice biomarker and diatom proxies from the Bering Sea show also substantial expansion in sea-ice through both glacials and interglacials from around 1.1 Ma, with seasonal advances and retreats of sea-ice controlling primary productivity (Detlef et al., 2018; Horikawa et al., 2015; Stroynowski et al., 2017; Teraishi et al., 2016). Larger amplitude SST variations are also observed after 1.1 Ma at Site U1425, in the Sea of Japan (Wittkopp et al., 2017). The increasing IRD accumulation rates and larger amplitude fluctuations in distal sites in the open ocean North Pacific ODP Site 887 and DSDP 580 since 1.2 Ma suggest a southward shift of the subarctic front (St. John and Krissek, 1999). Consequently, the rapid increase of *A. setosa* in several sites across the North Pacific and marginal seas corresponds to a cooling trend and is coincident with an increase in sea-ice and iceberg dynamics. This reflects that the FCO and early distribution of *A. setosa* was bound to the gradual expansion of polar waters and southward shift of the marginal ice zone, and supply of nutrients by melting ice across the North Pacific, being the Sea of Okhotsk the last region colonised. These conditions must have been similar to the Arctic and subpolar North Atlantic in which *A. setosa* is found today.

Despite the fact that *A. setosa* first appeared related to a climate cooling and a southward expansion of arctic conditions in the North Pacific, the distribution of *A. setosa* in Late Pleistocene sediments in the Sea of Okhotsk and Bering Sea is generally related to warm intervals and deglacial periods (Matul and Abelmann, 2005; Matul et al., 2002a). In core MD01-2415, located in the Sea of Okhotsk, high percentages of *A. setosa* (>30%) are observed during deglaciation at the same time or fairly closely following IRD discharge events a primary productivity proxies (opal and Diol index) MD01-2414 (Lattaud et al., 2019) (Fig. 7A–D). The Diol index is a proxy for the abundance of the diatom genus *Proboscia*, which in these settings is likely linked to nutrient availability (dissolved silica) (Lattaud et al., 2019). Deglacial productivity pulses in this region are controlled by a northward retreat of the sea-ice margins which allowed light to penetrate in the water column (Nürnberg and Tiedemann, 2004). These conditions together with higher nutrient (silica) concentration from the Amur River fluvial discharge, ice-rafting and vertical mixing promoted higher productivity (Iwasaki et al., 2012; Nürnberg and Tiedemann, 2004), favouring the presence of *A. setosa* in the Sea of Okhotsk. At Site SO201-2-77 KL, in the Bering Sea, the *A. setosa* record is very similar to those in the Sea of Okhotsk, and higher opal percentage at 125 ka (MIS 5e) coincides with a peak in *A. setosa* (>30%), indicating that productivity is controlled by analogous processes (Fig. 7E and F). The northward migration of the sea-ice edge and summer melt of marginal ice zones likely promoted upper ocean stratification, enough to foster a pulse of phytoplankton growth but not strong enough to prevent sustained growth via the resupply of nutrients from below (Kienast et al., 2004).

The preference of *A. setosa* for warmer climate intervals is illustrated by the robust negative correlation between downcore *A. setosa* abundances in the North Pacific since MIS 16 (~676 ka) and the $\delta^{18}O$ values of the benthic stack $\delta^{18}O$ (Lisiecki and Raymo, 2005), taken as an indication of global ice volume (Fig. 8A). That inverse relationship, which is observed in the Bering Sea and Sea of Okhotsk sites, suggests that a common mechanism driving *A. setosa* distribution was operating in both marginal basins and it is likely related to increased productivity at the marginal ice-zone. Exceptions are Sites U1425 and U1417. For the first one, in the Sea of Japan, the correlation between *A. setosa* and benthic $\delta^{18}O$ is positive. This is explained because Site U1425, as well as U1429 in the East China Sea, are located in a more southern position, and therefore optimal conditions for *A. setosa* (likely in the form of ice-rafted for the U1429), reached those latitudes only during very cold glacials. For the second one, in the Gulf of Alaska, productivity pulses occurred during glacial and interglacial periods (Müller

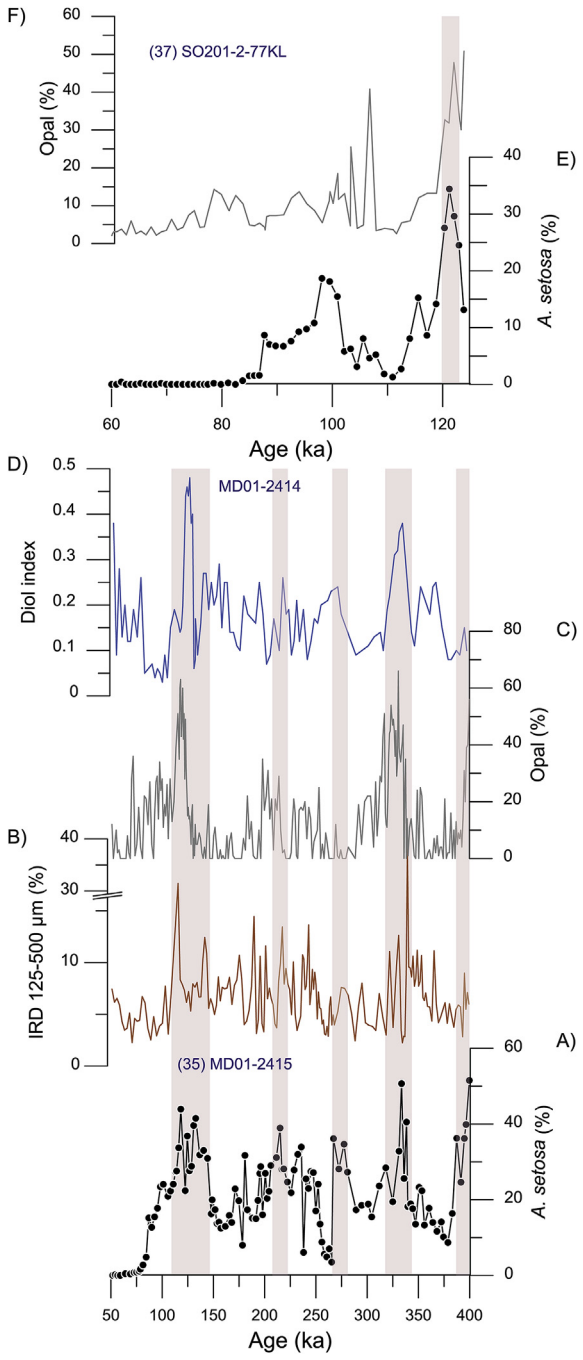

Fig. 7. (A) Downcore relative abundance of *A. setosa* (%) at site MD01-2415 (Matul et al., 2009), and (B) IRD 125–250 µm (%), (C) opal (%) and (D) Diol index from neighbouring Site MD01-2414) (Lattaud et al., 2019). (E) Downcore relative abundance of *A. setosa* (%) (this study), and (F) opal (%) (Riethdorf et al., 2013) at Site SO201-2-77 KL. Vertical red shading indicates peaks of *A.* setosa >30%. Numbers in parenthesis correspond to the code number in Table 3. (For interpretation of the references to colour in this figure legend, the reader is referred to the Web version of this article.)

et al., 2018), as well as the peaks in *A. setosa,* suggesting that local factors exert a major influence in the timing and extension of the ice-marginal zone in the Gulf of Alaska.

The interglacial signature observed in downcore records of *A. setosa* in the Bering Sea and Sea of Okhotsk contrast with the distribution in the high-latitude North Atlantic and Nordic Seas, which shows a positive correlation and thus preference for glacial conditions (Fig. 8A). Only a couple of sites located in the Norwegian Sea (GIK23424-3, GIK23259-2) do not show this positive correlation. This is explained because these sites only cover the last ca. 11 ka, and therefore benthic $\delta^{18}O$ values are <3.5‰, typical of interglacial conditions (McManus et al., 1999). In contrast to the Late Pleistocene-Holocene records, Mid- and Early Pleistocene records do not show a particular preference of this taxa for glacial or interglacial intervals (Fig. 8B, Sites U1417, U1341, U1425, and MD01-2415). Prior to the Mid-Pleistocene Transition (MPT), during the 41-kyr world (MIS 22–28), orbital climate variability does not show large amplitude changes (Clark et al., 2006). Biogeochemical proxies in the Bering Sea reveal that orbital fluctuations of the sea-ice margin were small during winter and summer (Detlef et al., 2018); therefore *A. setosa* could survive during either glacial or interglacial intervals, always being close to the ice margin. The onset of the 100-kyr glacial/interglacial cycles at the MPT is marked by a rapid transition from seasonal to perennial sea-ice conditions during glacials (Detlef et al., 2018) which decreased primary productivity (Kim et al., 2014; Nürnberg and Tiedemann, 2004), and limited the presence of *A. setosa* to interglacial and deglacial periods. We can conclude that the occurrence of *A. setosa* during either glacial or interglacial conditions across the Pleistocene in different parts of the Northern Hemisphere highlights the adaptive capacity of this species to follow spatial migrations of the marginal ice-zone and related factors (high productivity and low temperature) regardless of the global climate conditions (Fig. 9).

3.5.3. *The dawn of Amphimelissa setosa in the North Pacific*

High resolution records from the Bering Sea and Sea of Okhotsk show peaks of *A. setosa* during MIS 5e (123 ka), and also high values during MIS 5c (96 ka) and MIS 5a (82 ka). The relative abundance of *A. setosa* declined towards the beginning of MIS 4, until it finally disappeared from the North Pacific and its epicontinental seas (Fig. 10). The last occurrence (LO) of *A. setosa* is diachronous across the subarctic North Pacific. It disappeared earlier in the Sea of Okhotsk (e.g. MD01-2415) and the Gulf of Alaska (Site U1417), than in the Sea of Japan (Site U1425) and the Bering Sea (Site U1341) where *A. setosa* found a refuge (Table 3). Modern high-latitude North Pacific and North Atlantic basin differ in their upper water column oceanographic structure. Whereas the North Atlantic is well mixed, the North Pacific has strong salinity and temperature gradients in the uppermost 200 m, leading to a steep thermocline/halocline and pronounced stratification in the upper water column (Yang and Honjo, 1996) (Supplementary Figure 1). This stratification limits the supply of nutrients to the upper photic zone (Gargett, 1991). We suggest two non-exclusive mechanisms to explain the disappearance of *A. setosa* in the North Pacific basin: the development of perennial sea-ice conditions and shortages of silica. The increasing values of $\%C_{37:4}$ in the central Sea of Okhotsk since 85 ka are indicative of lower salinities (Seki et al., 2005) and reach their highest values at 64 ka coinciding with the LO of *A. setosa* in this marginal sea (Matul and Abelmann, 2005). The supply of large amounts of freshwater at the MIS 5a/4 transition from Amur River (Fig. 10K), in combination with lower SST (Hernandez-Almeida et al., 2020; Lattaud et al., 2019; Seki et al., 2004), promoted extension of the near-perennial sea-ice cover from west to east in the Sea of Okhotsk (Nürnberg et al., 2011; Sakamoto et al., 2005; Vasilenko et al., 2019). Abrupt changes in diatom $\delta^{30}Si$ and decreasing opal concentration were recorded at the MIS 5a/4 transition in the northwest Pacific, indicating a nutrient exhaustion or limited supply of silicic acid (Fig. 10K) linked to the establishment of a steep modern-like halocline (Swann and Snelling, 2015), which prevented deeper water mixing. Limitation in the nutrient renewal directly impacted the phytoplankton and caused a reduction primary productivity in the high-latitude North Pacific (Sancetta and Silvestri, 1986). Consequently, the anomalous

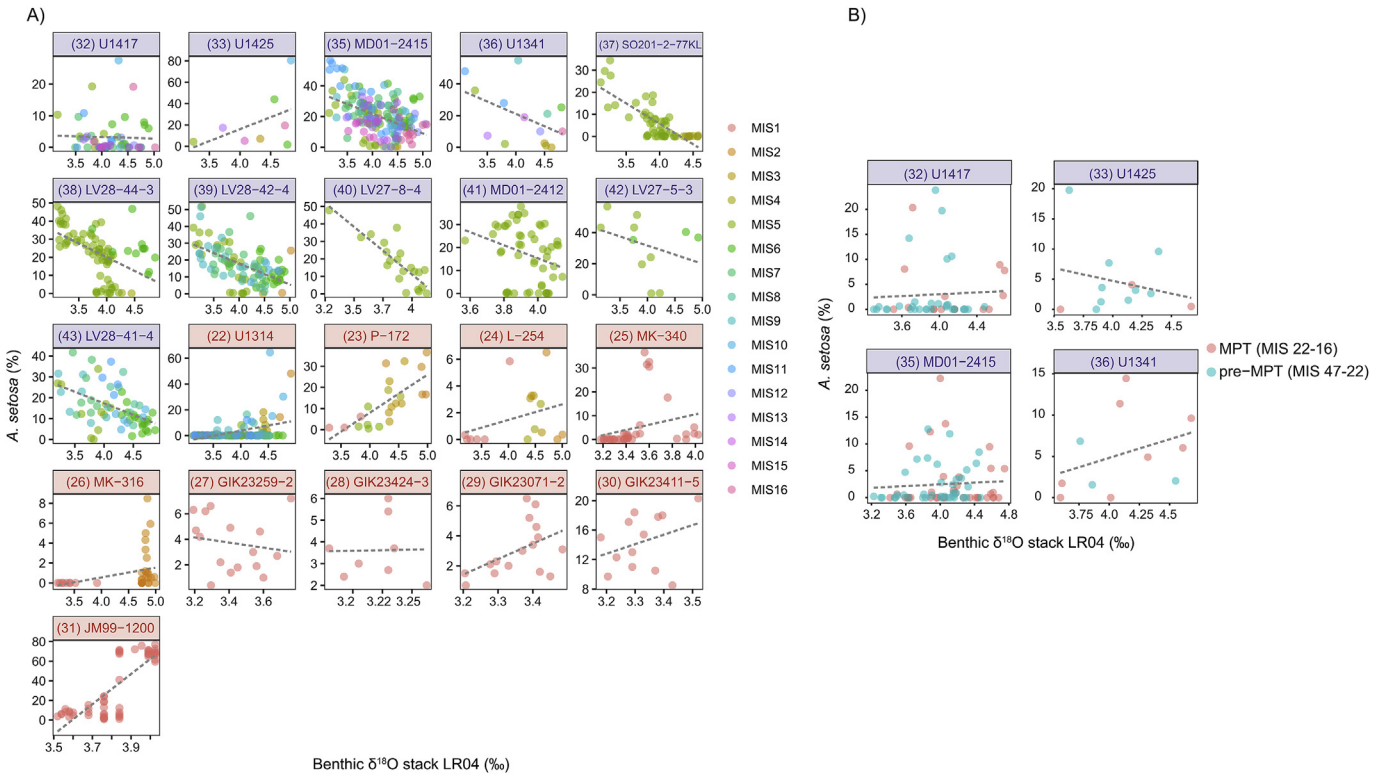

Fig. 8. Correlation between downcore *A. setosa* (%) relative abundances and the interpolated benthic $\delta^{18}O$ stack value for the respective age (Lisiecki and Raymo, 2005). Ages of the MIS follows Lisiecki and Raymo (2005). (A) Relative abundance of *A. setosa* data from different sites between MIS 16–1, and (B) sites with data corresponding to MPT (MIS 22–16) and pre-MPT (MIS 47–22) intervals. Grey dashed lines indicate the regression line between *A. setosa* relative abundances and benthic stack $\delta^{18}O$. Headers in red correspond to sites in North Atlantic, and in purple to the North Pacific. Numbers in parenthesis correspond to the code number in Table 3. (For interpretation of the references to colour in this figure legend, the reader is referred to the Web version of this article.)

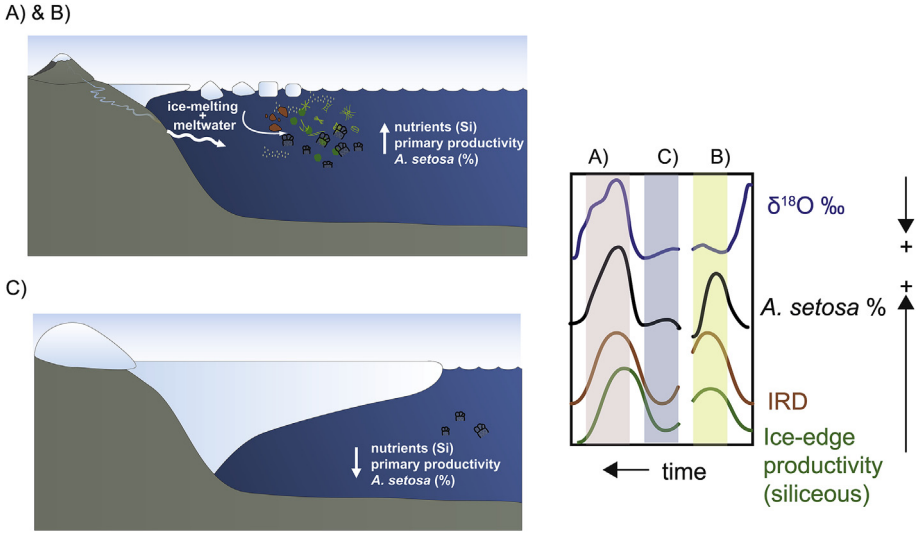

Fig. 9. Schematic description of the processes triggering high/low abundance of *A. setosa*. (A) Deglacial/interglacial scenarios in the Sea of Okhotsk and Bering Sea, and (B) IRD events during glacials in the North Atlantic: melting of glaciers and/or ice-melting supplies nutrients to the surface ocean, fueling productivity along the ice-edge. (C) Glacial scenarios in the Sea of Okhotsk and Bering Sea: perennial ice cover blocks light, and hampers mixing and upwelling of nutrients, limiting primary production.

formation of near-perennial sea-ice in the Sea of Okhotsk and/or the formation of a steep halocline in the high-latitude North Atlantic, caused a reduction in the main food-source of *A. setosa* (i.e., the phytoplankton thriving at the ice margins), which led to its decline and disappearance from the North Pacific basin.

4. Summary and outlook

Based on the extensive compilation of present-day, modern and fossil relative abundance data on the radiolarian species *Amphimelissa setosa* distributed across Greenland-Iceland Seas, Norwegian Sea, Labrador Sea and high-latitude North Atlantic and Arctic

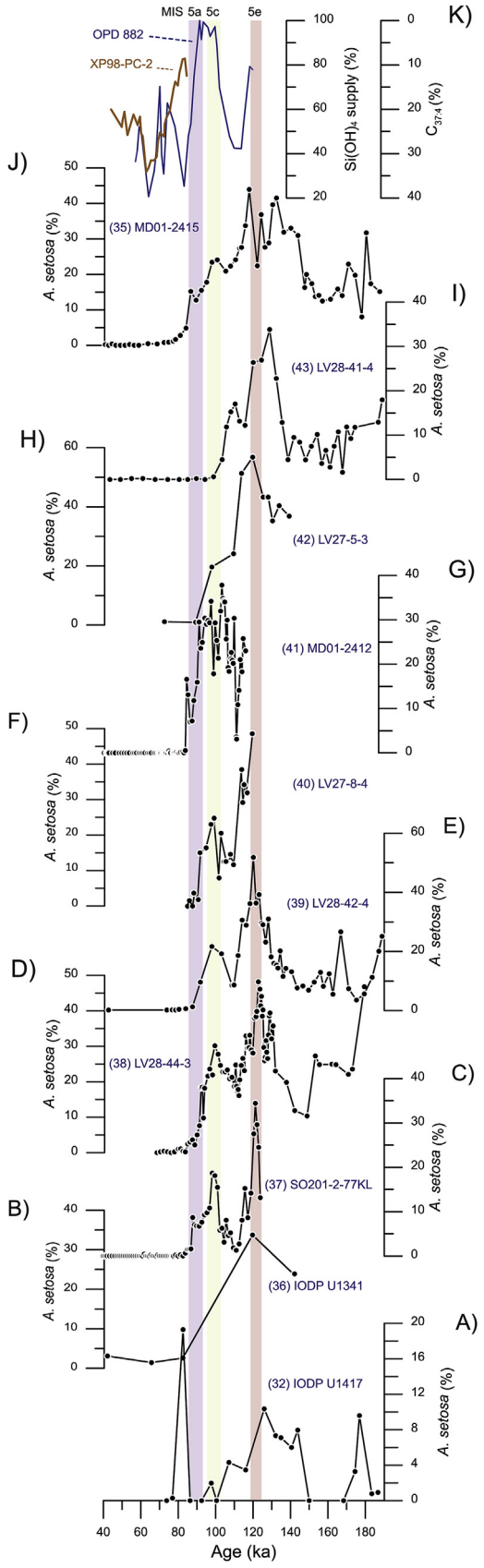

Fig. 10. Abundance of *A. setosa* in cores in the high-latitude North Pacific and marginal seas, between MIS 6 and 4. (A) IODP Site U1417 (Matsuzaki and Suzuki, 2018), (B) IODP Site U1341 (Ikenoue et al., 2016), (C) SO201-2-77 KL (this study), (D) LV28-44-3, (E) LV28-42-4 (F) LV27-8-4 (G) MD01-2412, (H) LV27-5-3 and (I) LV28-41-4 (Matul and Abelmann, 2005), (J) MD01-2415 (Matul et al., 2009). (J) Record of $C_{37:4}$ (%) at core XP98-PC2 (50.3°N, 148.2°E) (Seki et al., 2005) (brown line), and $Si(OH)_4$ supply (%) at ODP Site 882 (blue line) (50.3°N, 167.5°E) (Swann and Snelling, 2015) (note that vertical axis is inverted). Vertical red, yellow and purple shading indicate MIS 5e (123 ka), MIS 5c (96 ka) and MIS 5a (82 ka), respectively. Numbers in parenthesis correspond to the code number in Table 3. (For interpretation of the references to colour in this figure legend, the reader is referred to the Web version of this article.)

Oceans (including Chukchi and Beaufort Seas), we provide new insights into the potential of this species as a robust ecological proxy for past polar ocean temperature, salinity, nutrient (silica) and primary production conditions occurring at the ice-margin in the Northern Hemisphere.

At around 1.5–1 Ma atmospheric reorganization and enhanced polar circulation caused a southward sea-ice expansion, and a gradual development of the marginal ice zone in the entire North Pacific, with the Sea of Okhotsk being the last region consistently colonized by *A. setosa*. This taxon showed an exceptional adaptive capacity to follow the temporal and spatial migrations of the marginal ice zone and related factors (i.e., high primary productivity and low temperature) regardless of the global climate conditions. Prior to the MPT, *A. setosa* could survive close to the ice margin during either glacial or interglacial intervals. However, during MPT and Late Pleistocene *A. setosa* showed preference for interglacial and deglacial periods in records from the Bering Sea and Sea of Okhotsk, suggesting common mechanisms linked to the presence of sea-ice or ice-rafting.

The distribution of this species in the mid and late Pleistocene differ between ocean basins. The enhanced polar atmospheric circulation influenced by changes in ocean ice cover during MIS 4 promoted lower surface salinity, strong upper stratification and a decrease in productivity in the Sea of Okhotsk and high-latitude North Pacific. These conditions were intensified in the northwest Pacific, where the lack of a well-developed deep mixed layer and silica deprivation in the water column might have triggered the early disappearance of *A. setosa* in the subarctic Pacific. These conditions seem not have occurred in the high latitude North Atlantic Ocean, where this species migrated to and found a suitable habitat to dwell since MIS 11. There are large differences in size measurements between fossil and modern specimens of *A. setosa* in the Iceland Plateau, Norwegian Sea and high-latitude North Atlantic populations. Fossil individuals in downcore samples from the North Atlantic and the North Pacific show variations in morphological features. Differences are less marked between MIS 10 individuals from the North Atlantic and MIS 11–5 from the North Pacific, suggesting that genetic differentiation of ecological adaptation was very gradual. The differences in modern *A. setosa* populations reflect great endemism and genetic plasticity among the populations living in different parts of the North Atlantic Ocean. These morphological variations could be potential useful markers in future studies to trace differences in environmental parameters through time.

There are still unanswered questions regarding the modern and past ecological distribution of *A. setosa* in the high latitude oceans. Further studies investigating the occurrence of *A. setosa* in southern high-latitude locations, could help to better delimitate extension of sea-ice/ice-rafting in the high-latitude Northern Hemisphere. Moreover, lack of well-preserved opal records in the Arctic basin that cover the Middle and late Pleistocene limits the understanding of the inter-ocean migrations of *A. setosa*, which might have been analogous to other planktonic groups (e.g. *Neodenticula seminae*, Miettinen et al., 2013; Reid et al., 2007), and can shed light on the connection between North Pacific and North Atlantic during sea-level high stands, as well as changes in Arctic sea-ice cover.

Author statement

I.H.A designed research and analysed data; I.H.A. and N.S. performed research; T.I, K.R.B., A.M., N.S. and I.H.A. curated the data; I.H.A., K.R.B. wrote the paper; I.H.A., K.R.B., P.D., S.K., T.I., A.M., M.S–P. and N.S. commented, reviewed and edited the paper.

Data availability

All previously published and unpublished data are provided in Supplementary Materials and have been submitted to PANGAEA repository (https://www.pangaea.de/).

Declaration of competing interest

We wish to confirm that there are no known conflicts of interest associated with this publication and there has been no significant financial support for this work that could have influenced its outcome.

Acknowledgements

This research was funded by ETH Zürich. Thanks to the editor and three reviews for their comments, which greatly improved our manuscript. We are grateful to Lukas Jonkers and Mattia Greco for their help in the extraction of sea-ice data, and to Linda K. Eide for collecting processing and counting samples aboard Polarstern cruises. Mariem Saavedra-Pellitero was supported by the European Union's Horizon 2020 Research and Innovation Programme under the Marie Sklodowska-Curie grant agreement No 799531. Svetlana Kruglikova and Alexander Matul received support from the Shirshov Institute of Oceanology Project No. 0149-2019-0007.

Appendix A. Supplementary data

Supplementary data to this article can be found online at https://doi.org/10.1016/j.quascirev.2020.106565.

References

Abelmann, A., 1988. Freeze-drying simplifies the preparation of microfossils. Micropaleontology 34.
Abelmann, A., Brathauer, U., Gersonde, R., Sieger, R., Zielinski, U., 1999. Radiolarian-based transfer function for the estimation of sea surface temperatures in the Southern Ocean (Atlantic Sector). Paleoceanography 14, 410–421.
Akaike, H., 1973. Information theory as an extension of the maximum likelihood principle. In: Petrov, B.N., Csaki, F., Csaki, B.N.P.B.F. (Eds.), Second International Symposium on Information Theory. Academiai Kiado, Budapest.
Alvarez Zarikian, C.A., Stepanova, A.Y., Grützner, J., 2009. Glacial–interglacial variability in deep sea ostracod assemblage composition at IODP Site U1314 in the subpolar North Atlantic. Mar. Geol. 258, 69–87.
Anderson, O.R., Bryan, M., Bennett, P., 1990. Experimental and observational studies of radiolarian physiological ecology: 4. Factors determining the distribution and survival of Didymocyrtis tetrathalamus tetrathalamus with implications for paleoecological interpretations. Mar. Micropaleontol. 16, 155–167.
Anderson, O.R., Hays, J.D., Gross, M., 1988. An ontogenetic analysis of changes in morphology during phylogeny of some Lamprocyrtis spp. from deep sea sediments. Micropaleontology 34, 41–51.
Apollonio, S., 1973. Glaciers and nutrients in Arctic seas. Science 180, 491–493.
Assmy, P., Ehn, J.K., Fernández-Méndez, M., Hop, H., Katlein, C., Sundfjord, A., Bluhm, K., Daase, M., Engel, A., Fransson, A., 2013. Floating ice-algal aggregates below melting Arctic sea ice. PloS One 8.
Bendle, J., Rosell-Melé, A., Ziveri, P., 2005. Variability of unusual distributions of alkenones in the surface waters of the Nordic seas. Paleoceanography 20.
Biard, T., Ohman, M.D., 2020. Vertical Niche Definition of Test-Bearing Protists (Rhizaria) into the Twilight Zone Revealed by in Situ Imaging. Limnology and Oceanography in press.
Bitz, C., Gent, P., Woodgate, R., Holland, M., Lindsay, R., 2006. The influence of sea ice on ocean heat uptake in response to increasing CO_2. J. Clim. 19, 2437–2450.
Bjørklund, K.R., 1974. The seasonal occurrence and depth zonation of radiolarians in Korsfjorden, Western Norway. Sarsia 56, 13–42.
Bjørklund, K.R., Cortese, G., Swanberg, N., Schrader, H.J., 1998. Radiolarian faunal provinces in surface sediments of the Greenland, Iceland and Norwegian (GIN) Seas. Mar. Micropaleontol. 35, 105–140.
Bjørklund, K.R., Dumitrica, P., Dolven, J.K., Swanberg, N.R., 2008. Joergensenium rotatile n. gen., n. sp. (Entactinaria, Radiolaria): its distribution in west Norwegian fjords. Micropaleontology 53, 457–468.
Bjørklund, K.R., Hatakeda, K., Kruglikova, S.B., Matul, A.G., 2015. Amphimelissa setosa (Cleve)(Polycystina, Nassellaria)–a stratigraphic and paleoecological marker of migrating polar environments in the northern hemisphere during the quaternary. Stratigraphy 12, 23–37.
Bjørklund, K.R., Kruglikova, S.B., 2003. Polycystine radiolarians in surface sediments in the Arctic Ocean basins and marginal seas. Mar. Micropaleontol. 49, 231–273.
Bjørklund, K.R., Kruglikova, S.B., Hammer, Ø., 2019. The radiolarian fauna during the Younger Dryas–Holocene transition in Andfjorden, northern Norway. Polar Res. 38.
Bjørklund, K.R., Swanberg, N.R., 1987. The distribution of two morphotypes of the radiolaria *Amphimelissa setosa* Cleve (Nassellarida): a result of environmental variability? Sarsia 72, 245–254.
Boltovskoy, D., 2017. Vertical distribution patterns of Radiolaria Polycystina (Protista) in the World Ocean: living ranges, isothermal submersion and settling shells. J. Plankton Res. 1–20.
Boltovskoy, D., Correa, N., 2016. Biogeography of radiolaria polycystina (protista) in the World Ocean. Prog. Oceanogr. 149, 82–105.
Brown, W.L., Wilson, E.O., 1956. Character displacement. Syst. Zool. 5, 49–64.
Cabedo-Sanz, P., Belt, S.T., Knies, J., Husum, K., 2013. Identification of contrasting seasonal sea ice conditions during the Younger Dryas. Quat. Sci. Rev. 79, 74–86.
Carstens, J., Hebbeln, D., Wefer, G., 1997. Distribution of planktic foraminifera at the ice margin in the Arctic (Fram Strait). Mar. Micropaleontol. 29, 257–269.
Clark, P.U., Alley, R.B., Pollard, D., 1999. Northern Hemisphere ice-sheet influences on global climate change. Science 286, 1104–1111.
Clark, P.U., Archer, D., Pollard, D., Blum, J.D., Rial, J.A., Brovkin, V., Mix, A.C., Pisias, N.G., Roy, M., 2006. The middle Pleistocene transition: characteristics, mechanisms, and implications for long-term changes in atmospheric pCO2. Quat. Sci. Rev. 25, 3150–3184.
Cortese, G., Bjørklund, K.R., 1997. The morphometric variation of Actinomma boreale (Radiolaria) in Atlantic boreal waters. Mar. Micropaleontol. 29, 271–282.
Cortese, G., Bjørklund, K.R., Dolven, J.K., 2003. Polycystine radiolarians in the Greenland-Iceland-Norwegian Seas: species and assemblage distribution. Sarsia 88, 65–88.
Cortese, G., Dolven, J.K., Bjørklund, K.R., Malmgren, B.A., 2005. Late Pleistocene-Holocene radiolarian paleotemperatures in the Norwegian Sea based on artificial neural networks. Palaeogeogr. Palaeoclimatol. Palaeoecol. 224, 311–332.
Detlef, H., Belt, S.T., Sosdian, S.M., Smik, L., Lear, C.H., Hall, I.R., Cabedo-Sanz, P., Husum, K., Kender, S., 2018. Sea ice dynamics across the mid-pleistocene transition in the Bering Sea. Nat. Commun. 9, 941.
Dickson, R.R., Brown, J., 1994. The production of North Atlantic Deep Water: sources, rates, and pathways. J. Geophys. Res.: Oceans 99, 12319–12341.
Dittert, N., Baumann, K.H., Bickert, T., Henrich, R., Huber, R., Kinkel, H., Meggers, H., 1999. Carbonate dissolution in the deep-sea: methods, quantification and paleoceanographic application. In: Fischer, G., Wefer, G. (Eds.), Use of Proxies in Paleoceanography: Examples from the South Atlantic. Springer Berlin Heidelberg, Berlin, Heidelberg, pp. 255–284.
Dolan, J.R., Yang, E.J., Kim, T.W., Kang, S.-H.J.A.P., 2014. Microzooplankton in a Warming Arctic: A Comparison of Tintinnids and Radiolarians from Summer 2011 and 2012 in the Chukchi Sea, vol. 53.
Duprat, L.P., Bigg, G.R., Wilton, D.J., 2016. Enhanced Southern Ocean marine productivity due to fertilization by giant icebergs. Nat. Geosci. 9, 219–221.
Fryxell, G.A., 1989. Marine phytoplankton at the Weddell Sea ice edge: seasonal changes at the specific level. Polar Biol. 10, 1–18.
Garcia, H., Locarnini, R., Boyer, T., Antonov, J., Baranova, O., Zweng, M., Johnson, D., 2009. Dissolved oxygen, apparent oxygen utilization, and oxygen saturation. World Ocean Atlas 3.
Garcia, H., Locarnini, R., Boyer, T., Antonov, J., Baranova, O., Zweng, M., Reagan, J., Johnson, D., 2013. World ocean atlas 2013 ume 4, 1–25.
Gargett, A.E., 1991. Physical processes and the maintenance of nutrient-rich euphotic zones. Limnol. Oceanogr. 36, 1527–1545.
Gildor, H., Tziperman, E., 2000. Sea ice as the glacial cycles' climate switch: role of seasonal and orbital forcing. Paleoceanography 15, 605–615.
Greco, M., Jonkers, L., Kretschmer, K., Bijma, J., Kucera, M., 2019. Depth habitat of the planktonic foraminifera Neogloboquadrina pachyderma in the northern high latitudes explained by sea-ice and chlorophyll concentrations. Biogeosciences 16, 3425–3437.
Hadley, W., 2015. R Ggplot2 Package: an Implementation of the Grammar of Graphics. http://ggplot2.org.
Halbach, L., Assmy, P., Vihtakari, M., Hop, H., Duarte, P., Wold, A., Kauko, H.M., Kristiansen, S., Everett, A., Myhre, P.I., 2019. Tidewater glaciers and bedrock characteristics control the phytoplankton growth environment in an Arctic fjord. Frontiers in Marine Science 6, 254.
Harada, N., Shin, K.H., Murata, A., Uchida, M., Nakatani, T., 2003. Characteristics of alkenones synthesized by a bloom of emiliania huxleyi in the Bering Sea. Geochem. Cosmochim. Acta 67, 1507–1519.
Hawkings, J.R., Hatton, J.E., Hendry, K.R., de Souza, G.F., Wadham, J.L., Ivanovic, R., Kohler, T.J., Stibal, M., Beaton, A., Lamarche-Gagnon, G., 2018. The silicon cycle impacted by past ice sheets. Nat. Commun. 9, 1–10.
Hawkings, J.R., Wadham, J.L., Benning, L.G., Hendry, K.R., Tranter, M., Tedstone, A., Nienow, P., Raiswell, R., 2017. Ice sheets as a missing source of silica to the polar

oceans. Nat. Commun. 8, 14198.
Hernandez-Almeida, I., Boltovskoy, D., Kruglikova, S.B., Cortese, G., 2020. A new radiolarian transfer function for the pacific ocean and application to fossil records: assessing potential and limitations for the last glacial-interglacial cycle. Global Planet. Change, 103186.
Hopwood, M.J., Carroll, D., Dunse, T., Hodson, A., Holding, J.M., Iriarte, J.L., Ribeiro, S., Achterberg, E.P., Cantoni, C., Carlson, D.F., Chierici, M., Clarke, J.S., Cozzi, S., Fransson, A., Juul-Pedersen, T., Winding, M.H.S., Meire, L., 2020. Review article: how does glacier discharge affect marine biogeochemistry and primary production in the Arctic? Cryosphere 14, 1347–1383.
Horikawa, K., Martin, E.E., Basak, C., Onodera, J., Seki, O., Sakamoto, T., Ikehara, M., Sakai, S., Kawamura, K., 2015. Pliocene cooling enhanced by flow of low-salinity Bering Sea water to the Arctic Ocean. Nat. Commun. 6, 1–9.
Ikenoue, T., Bjørklund, K., Kruglikova, S., Onodera, J., Kimoto, K., Harada, N., 2015. Flux variations and vertical distributions of siliceous Rhizaria (Radiolaria and Phaeodaria) in the western Arctic Ocean: indices of environmental changes. Biogeosciences 12.
Ikenoue, T., Bjørklund, K.R., Fujiwara, A., Uchimiya, M., Kimoto, K., Harada, N., Nishino, S.J.P.B., 2019. Horizontal and vertical distribution of polycystine radiolarians in the western Arctic Ocean during the late summers of 2013 and 2015. Polar Biol. 42, 285–305.
Ikenoue, T., Okazaki, Y., Takahashi, K., Sakamoto, T., 2016. Bering Sea radiolarian biostratigraphy and paleoceanography at IODP Site U1341 during the last four million years. Deep Sea Res. Part II Top. Stud. Oceanogr. 125–126, 38–55.
Ingram, W., Wilson, C., Mitchell, J., 1989. Modeling climate change: an assessment of sea ice and surface albedo feedbacks. J. Geophys. Res.: Atmosphere 94, 8609–8622.
Ishii, M., Feely, R., Rodgers, K., Park, G.-H., Wanninkhof, R., Sasano, D., Sugimoto, H., Cosca, C., Nakaoka, S.-i., Telszewski, M., 2014. Air-sea CO2 flux in the pacific ocean for the period 1990-2009. Biogeosciences 11, 709–734.
Itaki, T., 2003. Depth-related radiolarian assemblage in the water-column and surface sediments of the Japan Sea. Mar. Micropaleontol. 47, 253–270.
Itaki, T., Ito, M., Narita, H., Ahagon, N., Sakai, H., 2003. Depth distribution of radiolarians from the Chukchi and Beaufort seas, western arctic. Deep-Sea Res. Part I Oceanogr. Res. Pap. 50, 1507–1522.
Iwasaki, S., Takahashi, K., Maesawa, T., Sakamoto, T., Sakai, S., Iijima, K., 2012. Paleoceanography of the last 500 kyrs in the central Okhotsk Sea based on geochemistry. Deep Sea Res. Part II Top. Stud. Oceanogr. 61–64, 50–62.
Jensen, S., 1998. Planktische Foraminiferen im Europäischen Nordmeer: Verbreitung und Vertikalfluß sowie ihre Entwicklung während der letzten 15000 Jahre. Christian-Albrechts-Universität Kiel.
Jin, M., Deal, C., Wang, J., Alexander, V., Gradinger, R., Saitoh, S.i., Iida, T., Wan, Z., Stabeno, P., 2007. Ice-associated phytoplankton blooms in the southeastern Bering Sea. Geophys. Res. Lett. 34.
Johannessen, T., Jansen, E., Flatøy, A., Ravelo, A.C., 1994. The Relationship between Surface Water Masses, Oceanographic Fronts and Paleoclimatic Proxies in Surface Sediments of the Greenland, Iceland, Norwegian Seas. Carbon cycling in the glacial ocean: constraints on the ocean's role in global change. Springer, pp. 61–85.
Kamikuri, S.-I., Itaki, T., Motoyama, I., Matsuzaki, K.M., 2017. Radiolarian biostratigraphy from middle miocene to late Pleistocene in the Japan sea. Paleontol. Res. 21, 397–421, 325.
Kandiano, E.S., Bauch, H.A., 2003. Surface ocean temperatures in the north-east Atlantic during the last 500 000 years: evidence from foraminiferal census data. Terra. Nova 15, 265–271.
Kienast, S.S., Hendy, I.L., Crusius, J., Pedersen, T.F., Calvert, S.E., 2004. Export production in the subarctic North Pacific over the last 800 kyrs: No evidence for iron fertilization? J. Oceanogr. 60, 189–203.
Kim, S., Takahashi, K., Khim, B.-K., Kanematsu, Y., Asahi, H., Ravelo, A.C., 2014. Biogenic opal production changes during the mid-pleistocene transition in the Bering Sea (IODP expedition 323 site U1343). Quat. Res. 81, 151–157.
Krause, G., Meincke, J., Schwarz, H., 1991. Scientific Cruise Reports of Arctic Expeditions ARK VI/1-4 of RV" Polarstern" in 1989, vol. 87. Berichte zur Polarforschung (Reports on Polar Research).
Kruglikova, S.B., Bjørklund, K.R., Hammer, Ø., Anderson, O.R., 2009. Endemism and speciation in the polycystine radiolarian genus Actinomma in the Arctic Ocean: description of two new species *Actinomma georgii* n. sp. and *A. turidae* n. sp. Mar. Micropaleontol. 72, 26–48.
Kruglikova, S.B., Bjørklund, K.R., Zasko, D.N., 2007. Distribution of polycystina (euradiolaria) in sediments and plankton of the arctic and marginal arctic seas. Dokl. Biol. Sci. 415, 284–287.
Lattaud, J., Lo, L., Zeeden, C., Liu, Y.-J., Song, S.-R., van der Meer, M.T., Damsté, J.S.S., Schouten, S., 2019. A multiproxy study of past environmental changes in the Sea of Okhotsk during the last 1.5 Ma. Org. Geochem. 132, 50–61.
Lisiecki, L.E., Raymo, M.E., 2005. A Pliocene-Pleistocene stack of 57 globally distributed benthic $\delta^{18}O$ records. Paleoceanography 20.
Locarnini, R., Mishonov, A., Antonov, J., Boyer, T., Garcia, H., Baranova, O., Zweng, M., Paver, C., Reagan, J., Johnson, D., Mishonov Technical, 2013. In: Levitus, S.A. (Ed.), World Ocean Atlas 2013, Volume 1: Temperature, vol. 73. NOAA Atlas NESDIS, p. 40.
Lumley, T., Lumley, M.T., 2013. Package 'leaps'. Regression Subset Selection. Thomas Lumley Based on Fortran Code by Alan Miller. Available online: http://CRAN.R-project.org/package=.leaps. (Accessed 18 March 2018).
Martínez-Garcia, A., Rosell-Melé, A., McClymont, E.L., Gersonde, R., Haug, G.H., 2010. Subpolar link to the emergence of the modern equatorial Pacific cold tongue. Science 328, 1550–1553.
Matsuoka, A., Anderson, O.R., 1992. Experimental and observational studies of radiolarian physiological ecology: 5. Temperature and salinity tolerance of Dictyocoryne truncatum. Mar. Micropaleontol. 19, 299–313.
Matsuzaki, K.M., Itaki, T., Tada, R., 2019. Paleoceanographic changes in the Northern East China Sea during the last 400 kyr as inferred from radiolarian assemblages (IODP Site U1429). Progress in Earth and Planetary Science 6, 22.
Matsuzaki, K.M., Itaki, T., Tada, R., Kamikuri, S.-i., Science, P., 2018. Paleoceanographic history of the Japan Sea over the last 9.5 million years inferred from radiolarian assemblages (IODP Expedition 346 Sites U1425 and U1430). Progress in Earth and Planetary Science 5, 54.
Matsuzaki, K.M., Suzuki, N., 2018. Quaternary radiolarian biostratigraphy in the subarctic northeastern Pacific (IODP Expedition 341 Site U1417) and synchroneity of bioevents across the North Pacific. J. Micropalaeontol. 37, 1–10.
Matul, A.G., Yushina, I.G., 1999. Radiolarians in north atlantic sediments. In: Spielhagen, R.F., Barash, M.S., Ivanov, G.I., Thiede, J. (Eds.), German-Russian Cooperation: Biogeographic and Biostratigraphic Investigations on Selected Sediment Cores from the Eurasian Continental Margin and Marginal Seas to Analyze the Late Quaternary Climatic Variability, pp. 35–45. Bremerhaven.
Matul, A., 1989. The distribution of radiolarians in the surface layer of North Atlantic bottom sediments. Oceanology 29, 740–745.
Matul, A., 1994. On the Late Quaternary paleoceanology of the North-Atlantic by the data of the radiolarian analysis. Okeanologiya 34, 607–613.
Matul, A., 1995. Late Quaternary paleoceanology of the North Atlantic based on radiolaria analysis data. Oceanol. Russ. Acad. Sci. 34, 550–555.
Matul, A., Abelmann, A., 2005. Pleistocene and Holocene distribution of the radiolarian Amphimelissa setosa cleve in the north pacific and North atlantic: evidence for water mass movement. Deep-Sea Res. Part II Top. Stud. Oceanogr. 52, 2351–2364.
Matul, A., Abelmann, A., Nürnberg, D., Tiedemann, R., 2009. Stratigraphy and major paleoenvironmental changes in the Sea of Okhotsk during the last million years inferred from radiolarian data. Oceanology 49, 93–100.
Matul, A., Abelmann, A., Tiedemann, R., Kaiser, A., Nürnberg, D., 2002a. Late Quaternary polycystine radiolarian datum events in the Sea of Okhotsk. Geo Mar. Lett. 22, 25–32.
Matul, A., Mohan, R., 2017. Distribution of polycystine radiolarians in bottom surface sediments and its relation to summer sea temperature in the high-latitude North Atlantic. Frontiers in Marine Science 4, 330.
Matul, A., Yushina, I., 1999. Radiolarians in north atlantic sediments. Ber. Polarforsch. 306, 35–45.
Matul, A., Yushina, I., Emelyanov, E., 2002b. On the Late Quaternary paleohydrological parameters of the Labrador Sea based on radiolarians. Okeanologiya 42, 247–251.
McClymont, E.L., Rosell-Melé, A., Haug, G.H., Lloyd, J.M., 2008. Expansion of subarctic water masses in the North Atlantic and Pacific oceans and implications for mid-Pleistocene ice sheet growth. Paleoceanography 23.
McManus, J.F., Oppo, D.W., Cullen, J.L., 1999. A 0.5-million-year record of millennial-scale climate variability in the North Atlantic. Science 283, 971–975.
Meire, L., Meire, P., Struyf, E., Krawczyk, D., Arendt, K., Yde, J., Juul Pedersen, T., Hopwood, M.J., Rysgaard, S., Meysman, F., 2016. High export of dissolved silica from the Greenland Ice Sheet. Geophys. Res. Lett. 43, 9173–9182.
Miettinen, A., Koç, N., Husum, K., 2013. Appearance of the Pacific diatom Neodenticula seminae in the northern Nordic Seas—an indication of changes in Arctic sea ice and ocean circulation. Mar. Micropaleontol. 99, 2–7.
Molina-Cruz, A., 1991. Holocene palaeo-oceanography of the northern Iceland Sea, indicated by Radiolaria and sponge spicules. J. Quat. Sci. 6, 303–312.
Molina-Cruz, A., Bernal-Ramírez, R.D., 1996. Distribution of Radiolaria in surface sediments and its relation to the oceanography of the Iceland and Greenland Seas. Sarsia 81, 315–328.
Montgomery, D., Peck, E., 1992. Introduction to Linear Regression Analysis. Wiley, New York, USA.
Müller, J., Romero, O., Cowan, E.A., McClymont, E.L., Forwick, M., Asahi, H., März, C., Moy, C.M., Suto, I., Mix, A., 2018. Cordilleran ice-sheet growth fueled primary productivity in the Gulf of Alaska, northeast Pacific Ocean. Geology 46, 307–310.
Nelson, R., Carmack, E., McLaughlin, F., Cooper, G., 2009. Penetration of Pacific zooplankton into the western Arctic Ocean tracked with molecular population genetics. Mar. Ecol. Prog. Ser. 381, 129–138.
Norris, R.D., 2000. Pelagic species diversity, biogeography, and evolution. Paleobiology 26, 236–258.
Nürnberg, D., Dethleff, D., Tiedemann, R., Kaiser, A., Gorbarenko, S.A., 2011. Okhotsk Sea ice coverage and Kamchatka glaciation over the last 350 ka—evidence from ice-rafted debris and planktonic δ18O. Palaeogeogr. Palaeoclimatol. Palaeoecol. 310, 191–205.
Nürnberg, D., Tiedemann, R., 2004. Environmental change in the Sea of Okhotsk during the last 1.1 million years. Paleoceanography 19.
Ogane, K., Tuji, A., Suzuki, N., Matsuoka, A., Kurihara, T., Hori, R.S., 2010. Direct observation of the skeletal growth patterns of polycystine radiolarians using a fluorescent marker. Mar. Micropaleontol. 77, 137–144.
Okazaki, Y., Takahashi, K., Katsuki, K., Ono, A., Hori, J., Sakamoto, T., Uchida, M., Shibata, Y., Ikehara, M., Aoki, K., 2005. Late Quaternary paleoceanographic changes in the southwestern Okhotsk Sea: evidence from geochemical, radiolarian, and diatom records. Deep-Sea Res. Part II Top. Stud. Oceanogr. 52, 2332–2350.
Pirrung, M., Fütterer, D., Grobe, H., Matthießen, J., Niessen, F., 2002. Magnetic

susceptibility and ice-rafted debris in surface sediments of the Nordic Seas: implications for Isotope Stage 3 oscillations. Geo Mar. Lett. 22, 1–11.
R Core Team, 2019. R: A Language and Environment for Statistical Computing. R Foundation for Statistical Computing. R version 3.6. 0.
Rayner, N., Parker, D.E., Horton, E., Folland, C.K., Alexander, L.V., Rowell, D., Kent, E., Kaplan, A., 2003. Global analyses of sea surface temperature, sea ice, and night marine air temperature since the late nineteenth century. J. Geophys. Res.: Atmosphere 108.
Rebotim, A., Voelker, A.H., Jonkers, L., Waniek, J.J., Meggers, H., Schiebel, R., Fraile, I., Schulz, M., Kucera, M., 2017. Factors controlling the depth habitat of planktonic foraminifera in the subtropical eastern North Atlantic. Biogeosciences 14, 827–859.
Reid, P.C., Johns, D.G., Edwards, M., Starr, M., Poulin, M., Snoeijs, P.J.G.C.B., 2007. A biological consequence of reducing Arctic ice cover: arrival of the Pacific diatom *Neodenticula seminae* in the North Atlantic for the first time in 800 000 years. Global Change Biol. 13, 1910–1921.
Riethdorf, J.-R., Nürnberg, D., Max, L., Tiedemann, R., Gorbarenko, S., Malakhov, M., 2013. Millennial-scale variability of marine productivity and terrigenous matter supply in the western Bering Sea over the past 180 kyr. Clim. Past 9, 1345–1373.
Ripley, B., Venables, B., Bates, D.M., Hornik, K., Gebhardt, A., Firth, D., Ripley, M.B., 2013. Package 'MASS'. Cran R 538.
Rosell-Melé, A., 1998. Interhemispheric appraisal of the value of alkenone indices as temperature and salinity proxies in high-latitude locations. Paleoceanography 13, 694–703.
Ruddiman, W.F., 1977. Late Quaternary deposition of ice-rafted sand in the subpolar North Atlantic (lat 40° to 65°N). GSA Bulletin 88, 1813–1827.
Sakamoto, T., Ikehara, M., Aoki, K., Iijima, K., Kimura, N., Nakatsuka, T., Wakatsuchi, M., 2005. Ice-rafted debris (IRD)-based sea-ice expansion events during the past 100 kyrs in the Okhotsk Sea. Deep Sea Res. Part II Top. Stud. Oceanogr. 52, 2275–2301.
Sancetta, C., Silvestri, S., 1986. Pliocene-pleistocene evolution of the north pacific ocean-atmosphere system, interpreted from fossil diatoms. Paleoceanography 1, 163–180.
Schlitzer, R., 2004. Export production in the equatorial and North Pacific derived from dissolved oxygen, nutrient and carbon data. J. Oceanogr. 60, 53–62.
Schlitzer, R., 2015. Ocean Data View.
Schlüter, M., Sauter, E.J., Schulz-Bull, D., Balzer, W., Suess, E., 2001. Fluxes of Organic Carbon and Biogenic Silica Reaching the Seafloor: A Comparison of High Northern and Southern Latitudes of the Atlantic Ocean, the Northern North Atlantic. Springer, pp. 225–240.
Schmidtko, S., Johnson, G.C., Lyman, J.M., 2013. MIMOC: a global monthly isopycnal upper-ocean climatology with mixed layers. J. Geophys. Res.: Oceans 118, 1658–1672.
Schröder-Ritzrau, A., 1995. Aktuopalaontologische Untersuchung zu Verbreitung und Vertikalfluss von Radiolarien sowie ihre raumliche und zeitliche Entwicklung im Europaischen Nordmeer. Berichte aus dem Sonderforschungsbereich 52, 99.
Schulz, H., 1995. Meeresoberflächentemperaturen vor 10.000 Jahren-Auswirkungen des frühholozänen Insolationsmaximums. In: Berichte-Reports, Geologisch-Paläontologisches Institut und Museum, Christian-Albrechts-Universität, Kiel, vol. 73, p. 119.
Seki, O., Kawamura, K., Ikehara, M., Nakatsuka, T., Oba, T., 2004. Variation of alkenone sea surface temperature in the Sea of Okhotsk over the last 85 kyrs. Org. Geochem. 35, 347–354.
Seki, O., Kawamura, K., Sakamoto, T., Ikehara, M., Nakatsuka, T., Wakatsuchi, M., 2005. Decreased surface salinity in the Sea of Okhotsk during the last glacial period estimated from alkenones. Geophys. Res. Lett. 32.
Sexton, P.F., Norris, R.D., 2008. Dispersal and biogeography of marine plankton: long-distance dispersal of the foraminifer Truncorotalia truncatulinoides. Geology 36, 899–902.
Siccha, M., Kucera, M., 2017. ForCenS, a curated database of planktonic foraminifera census counts in marine surface sediment samples. Scientific data 4, 170109.
St John, K., Flower, B.P., Krissek, L., 2004. Evolution of iceberg melting, biological productivity, and the record of Icelandic volcanism in the Irminger basin since 630 ka. Mar. Geol. 212, 133–152.
St John, K.E., Krissek, L.A., 1999. Regional patterns of Pleistocene ice-rafted debris flux in the North Pacific. Paleoceanography 14, 653–662.
Stroeve, J., Holland, M.M., Meier, W., Scambos, T., Serreze, M., 2007. Arctic sea ice decline: faster than forecast. Geophys. Res. Lett. 34.
Stroynowski, Z., Abrantes, F., Bruno, E., 2017. The response of the Bering Sea gateway during the mid-pleistocene transition. Palaeogeogr. Palaeoclimatol. Palaeoecol. 485, 974–985.
Sugiyama, K., Anderson, O.R., 1997. Experimental and observational studies of radiolarian physiological ecology, 6. Effects of silicate-supplemented seawater on the longevity and weight gain of spongiose radiolarians Spongaster tetras and Dictyocoryne truncatum. Mar. Micropaleontol. 29, 159–172.
Suzuki, N., Not, F., 2015. Biology and Ecology of Radiolaria, Marine Protists. Springer, pp. 179–222.
Suzuki, N., Ogawa, K., Ogane, K., Tuji, A., 2013. Patchwork silicification and disposal activity of siliceous fragments of a polycystine radiolarian. Rev. Micropaleontol. 56, 63–74.
Swanberg, N.R., Bjørklund, K.R., 1986. The radiolarian fauna of western Norwegian fjords; patterns of abundance in the plankton. Mar. Micropaleontol. 11, 231–241.
Swanberg, N.R., Bjørklund, K.R., 1987a. The pre-cephalic development of the skeleton of *Amphimelissa setosa* (Actinopoda; Nassellarida). Mar. Micropaleontol. 44, 333–341.
Swanberg, N.R., Bjørklund, K.R., 1987b. Radiolaria in the plankton of some fjords in western and northern Norway: the distribution of species. Sarsia 72, 231–244.
Swanberg, N.R., Bjørklund, K.R., 1992. The radiolarian fauna of western Norwegian fjords: a multivariate comparison of the sediment and plankton assemblages. Micropaleontology 38, 57–74.
Swanberg, N.R., Eide, L.K., 1992. The radiolarian fauna at the ice edge in the Greenland Sea during summer, 1988. J. Mar. Res. 50, 297–320.
Swann, G., Snelling, A.M., 2015. Photic zone changes in the north-west Pacific Ocean from MIS 4–5e. Clim. Past 11.
Swift, J.H., Aagaard, K., 1981. Seasonal transitions and water mass formation in the Iceland and Greenland seas. Deep Sea Research Part A. Oceanographic Research Papers 28, 1107–1129.
Syvertsen, E.E., 1991. Ice algae in the Barents Sea: types of assemblages, origin, fate and role in the ice-edge phytoplankton bloom. Polar Res. 10, 277–288.
Teraishi, A., Suto, I., Onodera, J., Takahashi, K., 2016. Diatom, silicoflagellate and ebridian biostratigraphy and paleoceanography in IODP 323 Hole U1343E at the Bering slope site. Deep Sea Res. Part II Top. Stud. Oceanogr. 125–126, 18–28.
Titchner, H.A., Rayner, N.A., 2014. The Met Office Hadley Centre sea ice and sea surface temperature data set, version 2: 1. Sea ice concentrations. J. Geophys. Res.: Atmosphere 119, 2864–2889.
Varela, D., Brzezinski, M., Beucher, C., Jones, J., Giesbrecht, K., Lansard, B., Mucci, A., 2016. Heavy silicon isotopic composition of silicic acid and biogenic silica in Arctic waters over the Beaufort shelf and the Canada Basin. Global Biogeochem. Cycles 30, 804–824.
Vasilenko, Y., Gorbarenko, S., Bosin, A., Artemova, A., Yanchenko, E., Shi, X.-F., Zou, J.-J., Liu, Y.-G., Toropova, S., 2019. Orbital-scale changes of sea ice conditions of Sea of Okhotsk during the last glaciation and the Holocene (MIS 4–MIS 1). Palaeogeogr. Palaeoclimatol. Palaeoecol. 533, 109284.
Walsh, J., 1978. A data set on Northern Hemisphere sea ice extent. Glaciological Data, Report GD 2, 49–51.
Weckström, K., Roche, B.R., Miettinen, A., Krawczyk, D., Limoges, A., Juggins, S., Ribeiro, S., Heikkilä, M., 2020. Improving the paleoceanographic proxy tool kit – on the biogeography and ecology of the sea ice-associated species Fragilariopsis oceanica, Fragilariopsis reginae-jahniae and Fossula arctica in the northern North Atlantic. Mar. Micropaleontol. 157, 101860.
Wittkopp, F., Yamamoto, M., Moossen, H., Dunkley Jones, T., Henderson, A.C.G.H., Bendle, J.A., 2017. Sea Surface Temperature Estimates for Sediment Cores in the Japan Sea. PANGAEA.
Yang, J., Honjo, S., 1996. Modeling the near-freezing dichothermal layer in the Sea of Okhotsk and its interannual variations. J. Geophys. Res.: Oceans 101, 16421–16433.
Zhang, Q., Chen, M., Zhang, L., Wang, R., Xiang, R., Hu, W., 2014. Radiolarian biostratigraphy in the southern Bering Sea since Pliocene. Sci. China Earth Sci. 57, 682–692.
Zweng, M.M., Reagan, J.R., Antonov, J.I., Locarnini, R.A., Mishonov, A.V., Boyer, T.P., Garcia, H.E., Baranova, O.K., Johnson, D.R., Seidov, D., 2013. World Ocean Atlas 2013, vol. 2. salinity.